nature medicine

Article

https://doi.org/10.1038/s41591-025-03562-5

Prospective, multicenter validation of a platform for rapid molecular profiling of central nervous system tumors

Received: 28 March 2024

Accepted: 4 February 2025

Published online: 25 March 2025

Check for updates

A list of authors and their affiliations appears at the end of the paper

Molecular data integration plays a central role in central nervous system (CNS) tumor diagnostics but currently used assays pose limitations due to technical complexity, equipment and reagent costs, as well as lengthy turnaround times. We previously reported the development of Rapid-CNS^2, an adaptive-sampling-based nanopore sequencing workflow. Here we comprehensively validated and further developed Rapid-CNS^2 for intraoperative use. It now offers real-time methylation classification and DNA copy number information within a 30-min intraoperative window, followed by comprehensive molecular profiling within 24 h, covering the complete spectrum of diagnostically and therapeutically relevant information for the respective entity. We validated Rapid-CNS^2 in a multicenter setting on 301 archival and prospective samples including 18 samples sequenced intraoperatively. To broaden the utility of methylation-based CNS tumor classification, we developed MNP-Flex, a platform-agnostic methylation classifier encompassing 184 classes. MNP-Flex achieved 99.6% accuracy for methylation families and 99.2% accuracy for methylation classes with clinically applicable thresholds across a global validation cohort of more than 78,000 frozen and formalin-fixed paraffin-embedded samples spanning five different technologies. Integration of these tools has the potential to advance CNS tumor diagnostics by providing broad access to rapid, actionable molecular insights crucial for personalized treatment strategies.

CNS tumors represent a particularly diverse and hard-to-treat group of cancers. Recent successes in clinical trials for targeted therapies address mutations or gene fusions in addition to traditional predictive markers such as *MGMT* promoter (*MGMT*p) methylation[1–4]. Among notable advancements in molecular diagnostics, the Heidelberg Molecular Neuropathology (MNP) methylation classifier (https://www.molecularneuropathology.org) has emerged as a pivotal diagnostic tool with more than 140,000 uploads to the website[5,6]. The 2021 World Health Organization (WHO) classification of CNS tumors (CNS5) underscores a paradigm shift toward the evaluation of a wide range of molecular alterations, including methylation-based classification, to report WHO-compatible integrated diagnoses[7]. Conventional state-of-the-art workflows necessitate substantial investment, are labor intensive and require batching of samples, which result in turnaround times in the order of several days or weeks[8,9]; this has consequently confined them to institutions with high-throughput capabilities.

In the dynamic field of CNS tumor diagnostics, there is a growing demand for methodologies that are comprehensive as well as rapid and accessible. In fact, the multitude of biomarkers necessary for

e-mail: m.sill@kitz-heidelberg.de; felix.sahm@med.uni-heidelberg.de

WHO-conformant diagnostics in the CNS5 classification has provoked criticism for being incompatible with the WHO's mandate to consider needs worldwide[10].

Nanopore sequencing is rapidly emerging as an efficient technique for rapid and cost-effective DNA sequencing. Its distinctive feature of directly reading native DNA enables the acquisition of genetic and epigenetic information in a single assay, thus eliminating the need for separate workflows. Several approaches have been described to enable swift and even intraoperative methylation classification using sparse nanopore sequencing data[11–16]. However, these approaches do not report targetable alterations, particularly mutation and fusion data. A noteworthy attribute of nanopore sequencing is the capability to reverse the voltage across pores, a process referred to as adaptive sampling. Unlike traditional sequencing methods that rely on capture or amplicon approaches, this permits the selection of molecules for sequencing based on real-time assessment of a small initial part of the reads[17]. Leveraging readfish[18], a tool developed to enable genome-level adaptive sampling, with CNS tumor relevant targets, we previously published a technical proof-of-concept study for our platform Rapid-CNS^2 (ref. 19). Yet, Rapid-CNS^2 provides granularity up to only 91 classes, whereas the latest version of the MNP classifier discriminates 184 (sub) classes. However, the current MNP classifier only accepts methylation array data as input. To overcome these limitations, we also developed MNP-Flex (https://mnp-flex.org), which classifies 184 categories from diverse sources. Here we present a combined workflow that allows for rapid stratification followed by high-resolution profiling (Fig. 1a) and introduces platform-independent methylation classification with the most up-to-date granularity (Fig. 1b).

Results

Next-day reporting of molecular diagnostic results

After a proof-of-concept preliminary version[19], Rapid-CNS^2 was run independently at two centers on fresh or cryopreserved tumor tissue (University Hospital Heidelberg, Germany and University of Nottingham, United Kingdom). We provided a comprehensive report to the neuropathologist including quality control (QC) parameters, clinically relevant single nucleotide variants (SNVs), small insertions and deletions (Indels), gene fusions or structural variants (SVs), copy number variations (CNVs), *MGMT* promoter methylation status and methylation classification to make a WHO-compatible integrated diagnosis. All sequencing and analysis conditions are described in Supplementary Table 1. The pipeline can be run on the MinION, GridION and PromethION devices, as well as the new R10 flow cells. To establish and test the feasibility of varied sequencing conditions, we sequenced archived frozen tissue from 112 samples using the Rapid-CNS^2 pipeline at the Department of Neuropathology, Heidelberg. In parallel, we prospectively sequenced DNA from fresh tissue sent to the Department of Neuropathology, Heidelberg and issued comprehensive molecular diagnostic reports in a real diagnostic setting for 140 patient samples. Once the pipeline was set up for regular prospective application, 51 of 62 CNS tumor samples (82.3%) sent between February and May 2024 underwent the Rapid-CNS^2 pipeline without any restrictions on tissue amount or quality (Supplementary Table 1). We achieved an average turnaround time of 2 days from tissue receipt to complete report (methylation classification, CNVs, SNVs and/or Indels, SVs) for diagnostic samples compared with an average of 20 days for the conventional workflow. When subtracting avoidable logistical and organizational delays, the entire pipeline took only 40 h. Similarly, Rapid-CNS^2 was run on 27 archival and 22 prospective diagnostic samples at the University of Nottingham with an average turnaround time of 30 h as opposed to over several weeks for the conventional workflow. Among the wide scope of tumor types in our dataset, the cohort also included 74 molecular low-grade glial and glioneuronal tumors, 15 recurrent tumors, 10 samples with infiltration zones of diffuse glioma and 5 samples the size of a small biopsy (~1.5 mm diameter) (Supplementary Table 1).

In our attempt to scrutinize the workflow on an utmost diverse basis, we prospectively included 31 cases that in retrospect could not have been resolvable by methylation (for example, brain metastases, not represented in the CNS tumor methylation classifier). Yet, these were not censored in further analyses to provide a comprehensive picture of the performance.

Rapid-CNS^2 is available as a Nextflow pipeline that can be easily deployed with a single command and requires only a basic knowledge of command-line programming (https://github.com/areebapatel/Rapid-CNS2_nf).

Evaluation of reported molecular data

We integrated molecular alterations reported by Rapid-CNS^2 with conventional histopathology to issue WHO-compatible integrated diagnoses in a realistic diagnostic setting (Fig. 2). In addition, we compared each of the reported alterations separately with results from conventional methods. For 103 samples with matched next-generation sequencing (NGS) panel sequencing data, Rapid-CNS^2 accurately called 91.67% of the SNVs identified by NGS (Fig. 3a), well in line with established accuracy metrics between conventional sequencing and variant calling pipelines[20]. A minimum on-target coverage of 10X was required to achieve more than 90% concordance in mutation calls (Supplementary Fig. 1). Minor discordances between sequencing platforms are expected and are currently insurmountable given fundamental differences between long- and short-read technologies, but may become problematic if they persist in clinically relevant alterations. Hence, we further specifically investigated *IDH1/2* and *BRAF* mutations and found correct calling in 47 of 48 samples with matched NGS data and endorsed by direct sequencing and/or immunohistochemistry, with no false positives (97.9% sensitivity, 100% specificity). *MGMT* promoter methylation status reported by Rapid-CNS^2 considers the entire region as opposed to the two-site Bady model used for methylation arrays[21]. An unambiguous difference between the methylated and unmethylated tumor profiles could be identified (Fig. 3b). *MGMT* promoter status was concordant in 227 of 251 cases (90.4%) with matched *MGMT* predictions (Supplementary Fig. 2). This discrepancy is similar to that reported when comparing other *MGMT* methylation tests; for example, pyro-sequencing versus methylation array[22,23]. Of note, discrepancies in *MGMT* prediction are known to exist even among established, conventional methods, precluding definition of ground truth[8].

In addition, copy number profiles generated by Rapid-CNS^2 were in complete agreement with methylation array-generated counterparts in all 254 samples with corresponding Illumina Infinium Methylation BeadChip array (either 450K or EPIC) data available (Supplementary Fig. 3). Figure 3c shows an example of a glioblastoma sample with multiple focal alterations (highlighted), all of which were reproduced in the corresponding Rapid-CNS^2 profile. *KIAA1549:BRAF* fusion was accurately identified in all eight cases with that fusion established in conventional analysis and biologically supported by the type of tumor. Notably, this fusion was part of a 19-Mb duplication on chr. 7q34 with breakpoints in the introns of *BRAF* and *KIAA1549*, aligning with the proposed mechanism of tandem duplications in the region leading to the fusion[24] (Supplementary Fig. 4). Furthermore, as an example of the advantages of long-read sequencing, a subclonal 1.3-Mb deletion in *EGFR* spanning exons 2 to 7, known as *EGFR* vIII, was confidently detected in one glioblastoma sample with consistent breakpoint mapping[25]. Interestingly, this alteration had not been previously identified in NGS data, highlighting the advantage of long-read sequencing in SV detection (Supplementary Fig. 5).

Methylation classification using the built-in Rapid-CNS^2 model covers 91 CNS tumor classes from the MNP v.11 model[5]: Of 270 samples classifiable using conventional methods, 251 (92.9%) were assigned to the correct methylation family, typically the decisive level in diagnostics. Because the conventional random forest classifier imposes a cutoff (0.9) for cases that should be deemed 'classifiable', we derived a

https://doi.org/10.1038/s41591-025-03562-5

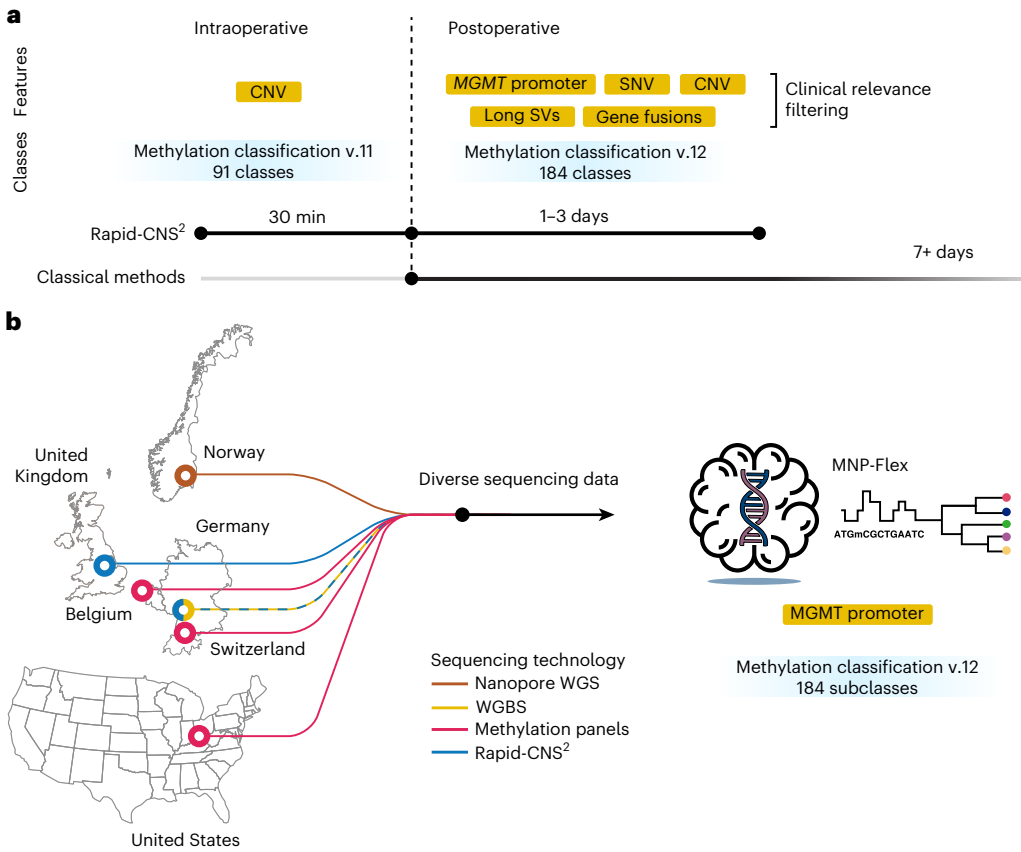

Fig. 1 | Overview of the Rapid-CNS^2 workflow and validation of MNP-Flex. **a**, Streamlined workflow that starts with intraoperative sequencing to report broad methylation classification and arm-level copy number alterations followed by postoperative sequencing to report comprehensive molecular markers and fine-grained methylation classification. Lines below indicate the timeline for Rapid-CNS^2 versus classical methods. **b**, Sources and types of sequencing data used for validation of MNP-Flex. Credits: Brain outline in **b** adapted from SVG Repo (https://www.svgrepo.com) under a Creative Commons license CC BY 4.0; DNA helix adapted from SVG Repo (https://www.svgrepo.com) under a Creative Commons license CC BY 4.0. Signal and classification tree in the MNP-Flex logo in **b** was created using BioRender.com.

cutoff from the Rapid-CNS^2 data: on filtering samples with at least 30% confidence score, 221 of 230 (96.1%) samples were correctly predicted (Fig. 3d). However, to provide a comprehensive picture of performance, we included all cases irrespective of score. Even at the methylation class level, 164 of 223 samples (73.5%) with that information available were matching. For example, cases concordant on the family level, but not on the class level comprised 42 instances in the glioblastoma, *IDH* wild-type methylation family. Despite classes being available, granularity in glioblastoma, *IDH* wild-type, is not endorsed by the current WHO classification because of a lack of known clinical relevance and has even been shown to vary in a given sample[26,27]. The latter may well explain the difference at the class level between frozen and formalin-fixed paraffin-embedded (FFPE) fragments in some cases.

While 8 of the 19 nonmatching samples were predicted as compatible classes of 'inflammatory glioblastoma microenvironment' or 'reactive tumor microenvironment' unequivocal for glioblastoma or broader tumor context respectively, the remaining 11 samples were considered clear mismatches. Reassuringly, samples with correct predictions generally had higher scores than samples with mismatches or outside the reference set, indicating a conservative approach (Supplementary Fig. 6a).

Integrated diagnoses leveraging all layers of molecular data generated by Rapid-CNS^2 in 285 of 301 (94.6%) cases were in complete accordance with corresponding integrated diagnoses obtained through conventional methods, affirming the reliability of Rapid-CNS^2 in providing accurate and comprehensive diagnostic information for CNS tumors (Extended Data Fig. 1). The added value beyond methylation in rendering a precise diagnosis encompassed pathognomonic CNVs (for example, 7/10 in glioblastoma, 1p/19q in oligodendroglioma), mutations (for example, *IDH1*, *TERT*) and/or gene fusions (for example, *KIAA1549::BRAF*) to distinguish between differential diagnoses in cases not resolved by methylation alone. Remarkably, all small biopsy, recurrence and infiltration zone samples could be issued concordant integrated diagnosis (Supplementary Table 1). Four of the 16 discordant cases were compatible with but not identical to the conventional integrated diagnosis. Seven others would have benefited from the granularity of a fine-grained version of the CNS classifier, v.12. In only 5 of 301 cases (1.6%), were the data from Rapid-CNS^2 potentially misleading. This is well in line with the rate in conventional array-based classification[5,28]. Notably, earlier studies defined cutoffs for 'classified' cases, whereas this analysis includes all samples regardless of score, still yielding a low error rate. Importantly, none of them presented a consistent picture of a confident but incorrectly called diagnosis, but evidently called for additional analysis in keeping with the integrated diagnosis concept of the WHO classification. As opposed to separately and sequentially run molecular assays, the concurrent availability of all data layers in Rapid-CNS^2 increases procedural safety for patients.

Illustrative of the advantages is, for example, one case (Study ID 212) in which a glioma was initially suspected based on smear and frozen section analysis. However, Rapid-CNS^2 identified it as an Ewing family tumor with a capicua transcriptional repressor gene (*CIC*) alteration. Similarly, MNP-Flex predicted it to be a *CIC*-rearranged sarcoma, aligning with the eventually available methylation array

https://doi.org/10.1038/s41591-025-03562-5

Fig. 2 | Overview of concordance for the Rapid-CNS² cohort. a, Archival samples. **b**, Diagnostic samples. Bars indicate on-target coverage, sequencing time and the percentage of SNVs that were recovered in Rapid-CNS² data from their corresponding NGS data. Site and device blocks indicate site of sequencing (University Hospital Heidelberg or University of Nottingham) and the device that sequencing was run on. NGS and methylation array blocks indicate the availability of corresponding conventional data. Following blocks indicate concordance with available matched conventional data. Methylation classification displays concordance levels of the Rapid-CNS² ad hoc classifier with corresponding methylation array-based classification. Methylation class indicates the 'ground truth' or inferred methylation class. *MGMT*p shows concordance of *MGMT* promoter methylation status with matched conventional data.

prediction. Markedly, integrated diagnosis with Rapid-CNS² was established within 5 days without prioritization, whereas it took 1 month with conventional methods (Extended Data Fig. 2). Considering the aggressive nature of these tumors, an early diagnosis is essential for swift treatment.

Platform-agnostic methylation classifier for CNS tumors

With the surge in popularity of sequencing-based approaches for methylation calling, we aimed to widen the utility of the most recent MNP classifier version (v.12), hereafter referred to as MNP-RF. The MNP v.12 classifier follows a hierarchical scheme and includes 184 subclasses, 143 classes, 75 families and 34 superfamilies. To achieve this, we developed MNP-Flex—a platform-agnostic CNS tumor methylation classifier. We trained a gradient-boosted model that uses binarized methylation values to compensate for the nuances of the respective technologies used[29]. We tested this model on the entire MNP dataset consisting of more than 90,000 samples. The array test dataset included 48,598 (61.7%) FFPE and 30,174 (38.3%) cryopreserved samples for which sample type information was available. Generally, samples with scores ≥0.9 are considered to be reliably classified by the RF model[5,30]. Hence, we applied this cutoff as a criterion to include samples in the validation analysis, considering cases with scores ≥0.9 as ground truth.

https://doi.org/10.1038/s41591-025-03562-5

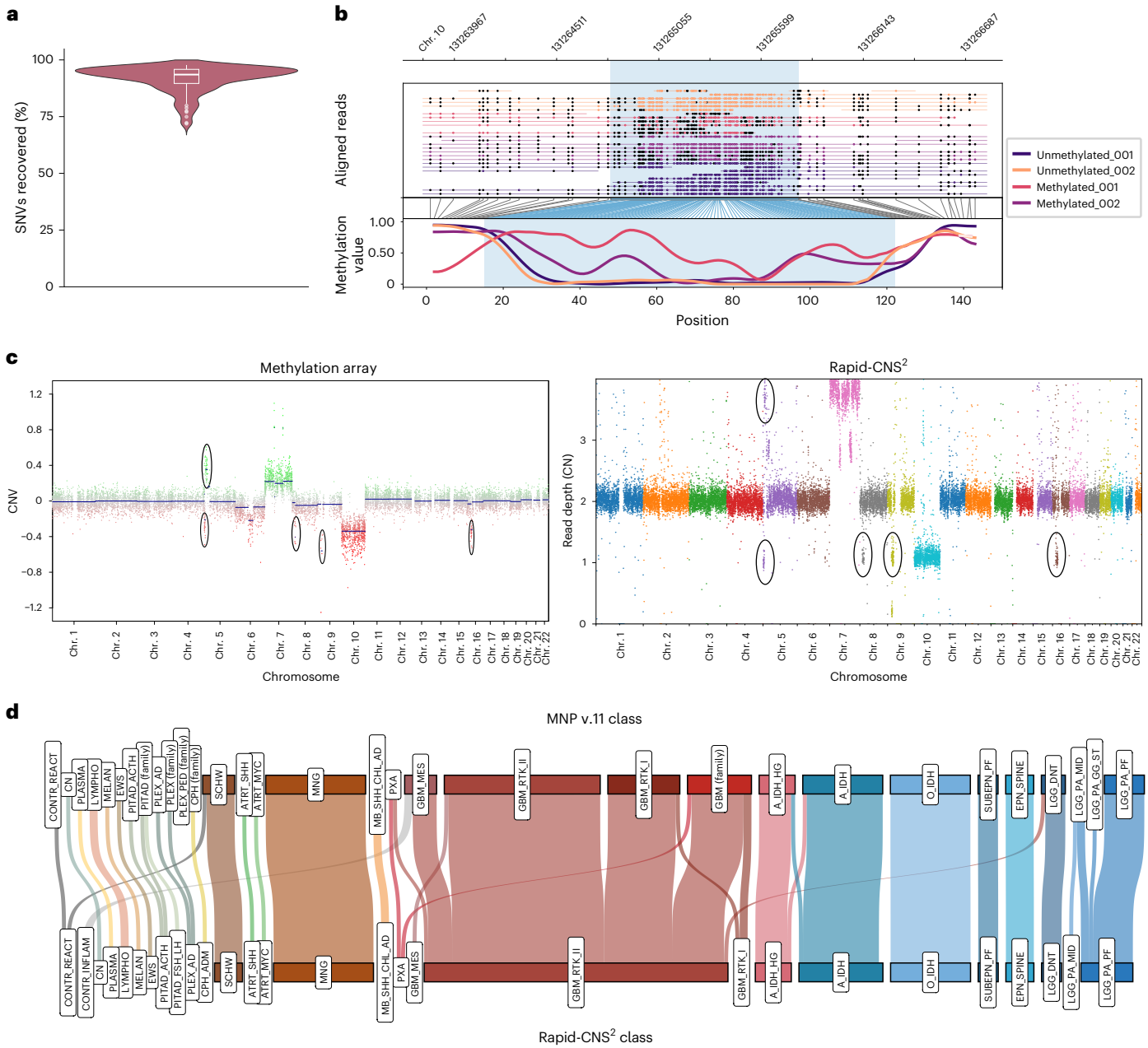

Fig. 3 | Evaluation of molecular markers reported by Rapid-CNS². **a**, Violin plot showing the percentage of SNVs recovered by Rapid-CNS² libraries compared with their corresponding NGS panel sequencing libraries ($n = 103$), with the width proportional to the frequency of values at each level. The overlaid box plot indicates the median (horizontal line), the 25th and 75th percentiles (edges of the box) and whiskers extending up to 1.5× the interquartile range from the box boundaries. Data points lying beyond these whisker bounds are shown individually as outliers. **b**, Methylation values of methylated and unmethylated glioblastoma samples over the *MGMT* promoter region (highlighted in blue). The panels show (top to bottom) aligned reads colored by sample with CpG sites marked as closed (methylated) or open (unmethylated) dots followed by smoothed methylation profiles for each sample. The smoothed profiles show a clear difference in overall methylation between methylated and unmethylated samples. **c**, CNV profile generated using EPIC array data (left) and CNV profile generated by Rapid-CNS² (right) for the same sample; focal alterations detected in both are highlighted with ovals. **d**, Sankey plot comparing predictions from the MNP v.11 classifier for methylation array data with the predictions by Rapid-CNS² (calibrated score >30%) for the same cases.

However, the 0.9 cutoff excludes a considerable number of cases in a real-world setting and is therefore suggested to be lowered in the literature; for example, to 0.84 (ref. 31). To account for this, in parallel, we considered a lower cutoff for MNP-RF of ≥0.7. As shown in Extended Data Table 1, we observed an increase in accuracy with higher cutoffs, ultimately achieving 99.3% subclass-level accuracy and 99.7% family-level accuracy with clinically applicable thresholds. In 176 of 182 subclasses, F_1 scores >0.5 were found, whereas 163 subclasses had F_1 scores ≥0.9 (Fig. 4a). Subclasses with low F_1 scores consisted of those with a low number of reference samples (Supplementary Fig. 7). To evaluate the variety of data sources, we tested MNP-Flex on a total of 448 samples with sequencing-based data covering 80 whole-genome bisulfite sequencing (WGBS), 27 methylation panels, 40 nanopore Oxford Nanopore Technologies whole-genome sequencing (ONT-WGS) and 301 Rapid-CNS² samples from seven institutes across the globe (Fig. 1). Sample-specific information is listed in Supplementary Table 2 and accuracies for each technology are indicated in Extended Data Table 1. Similar to the MNP-RF array classifier, we evaluated nonarray

https://doi.org/10.1038/s41591-025-03562-5

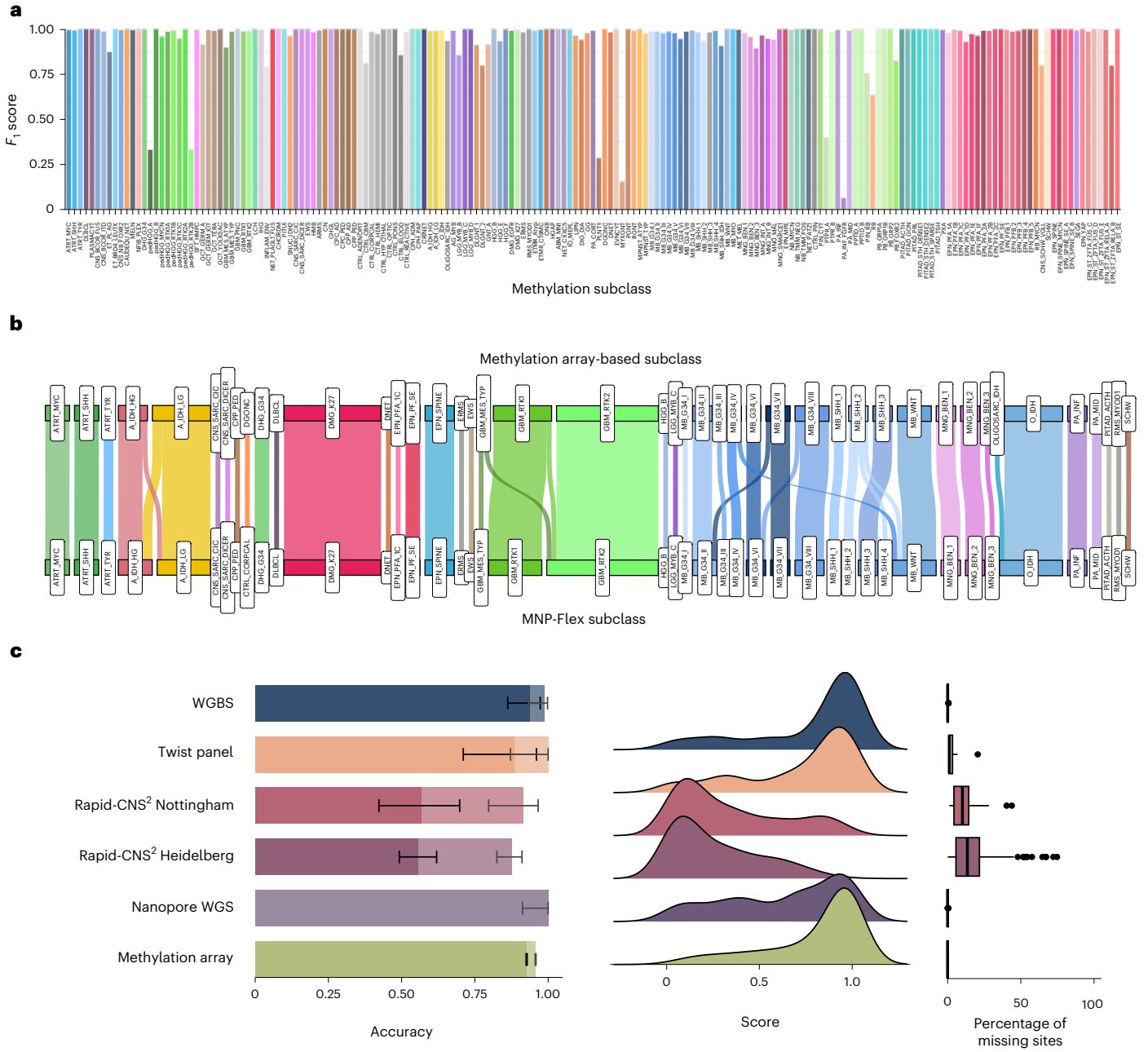

Fig. 4 | MNP-Flex validation. a, F_1 scores for the methylation array dataset comprising 78,833 samples covering 184 methylation classes. We considered the MNP random forest classifier as ground truth for comparison. All samples with an MNP-RF score >0.7 that were not included in the training set were used for validation. **b**, Sankey plot showing comparison of methylation array-based MNP-RF predictions with corresponding MNP-Flex predictions over the nonarray cohort. Only samples with an MNP-Flex prediction score >0.3 are shown. **c**, Comparison of MNP-Flex performance over different technologies. Bar plots indicate accuracy and error bars represent the 95% CIs calculated using a binomial proportion confidence interval via the binom.confint function in R. Samples were processed using WGBS ($n = 80$), Twist methylation panels ($n = 27$), nanopore adaptive-sampling-based Rapid-CNS^2 in Nottingham ($n = 41$) and Heidelberg ($n = 194$), ONT-WGS ($n = 40$) and the conventional methylation array ($n = 78,833$) dataset. Solid colored bars indicate subclass-level accuracy and bars with increased alpha indicate family-level accuracy. ONT-WGS samples did not have matched array predictions; thus, family-level predictions were inferred from histological and molecular findings. Density plots indicate scores for subclass prediction. Box plots denote percentage of missing CpG sites in each dataset. They include the median (horizontal line), with the box boundaries representing the 25th and 75th percentiles (interquartile range). Whiskers extend to 1.5× the interquartile range beyond the box limits. Data points beyond these whisker boundaries are plotted individually as outliers.

data to establish a cutoff score. Starting with a subclass accuracy of 65.9% and family accuracy of 91.9% for all nonarray samples without any cutoff, we observed an increase in subclass accuracy to 82.8% and in family accuracy to 99.5% on applying a prediction threshold of 0.3 (Extended Data Table 1 and Supplementary Fig. 8). Fraction of scores ≥0.3 did not significantly differ between frozen and FFPE samples (Supplementary Fig. 9). Figure 4b illustrates the distribution of ground truth and MNP-Flex predictions for samples with scores ≥0.3. In WGBS data, four misclassifications were in the same molecular family (for example, Medulloblastoma Group 4, subclass VIII classified as Medulloblastoma Group 4, subclass VI), while one diffuse intrinsic pontine glioma sample was predicted as 'inflammatory microenvironment'. For samples sequenced using Twist panels, one glioblastoma RTK1 subtype sample was classified as glioblastoma RTK2, while the other had limited

https://doi.org/10.1038/s41591-025-03562-5

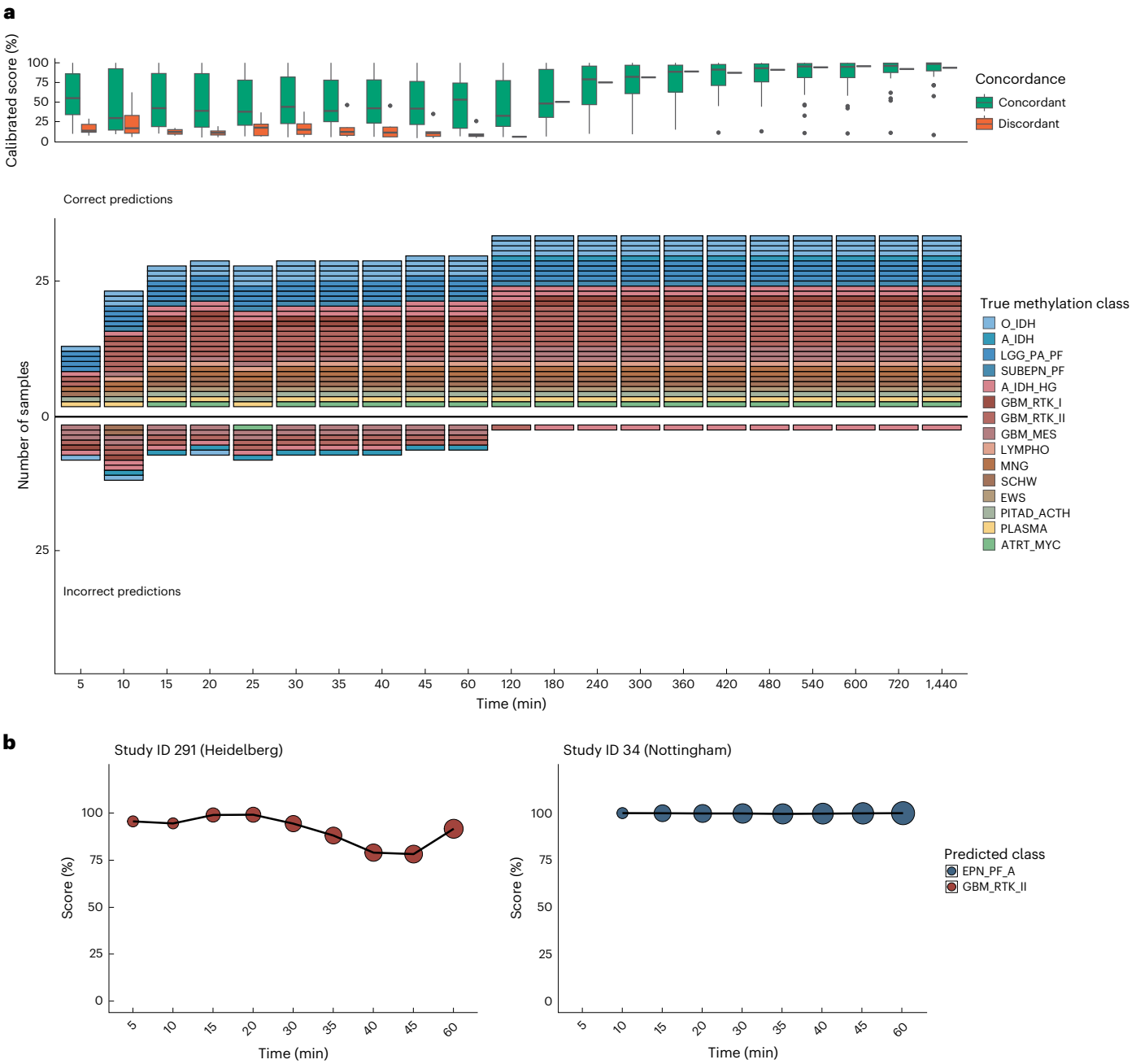

Fig. 5 | Intraoperative reporting. a, Box plots indicate calibrated scores for each time point for correct (green) and incorrect (orange) predictions for simulated retrospective samples. Box plots display the median (horizontal line) and the box boundaries represent the 25th and 75th percentiles (interquartile range). Whiskers extend to 1.5× the interquartile range beyond the box limits. Data points beyond the boundaries are plotted individually as outliers. The number of samples represented per box plot is equal to the number of samples indicated in the bar plots below. Bar plots indicate per-sample methylation class prediction concordance over time. Reads generated within the indicated sequencing time were used for analysis (top). Each rectangle on the bar plot indicates individual samples colored by ground truth methylation class from corresponding methylation array profiles. The *x* axis indicates time in minutes from beginning of sequencing. A positive *y* axis indicates correct predictions and a negative *y* axis indicates incorrect predictions (bottom). **b**, Prediction score versus time for intraoperative samples run in Heidelberg and Nottingham using a P2 Solo; color indicates class; size of dots indicates number of CpG sites.

sequencing reads and a very low prediction score ≤0.03. Because no array data were available, true methylation families were inferred for all ONT-WGS samples by taking into consideration reported molecular alterations and histological characteristics (Supplementary Table 2). Methylation classification by MNP-Flex was concordant for all ONT-WGS cases. The MNP-Flex model was not trained to account for large missingness in data. To test the native ability of the gradient-boosted model to make predictions on data with missing values, we tested it on samples sequenced using Rapid-CNS^2. Rapid-CNS^2 samples had an average of 16.6% missingness. In comparison, other methods had an average of <0.7% missing sites. After confidence filtering, we achieved 89.1% and 78% accuracy at the methylation subclass level, and 98.7% and 100% at the methylation family level for the Heidelberg and Nottingham Rapid-CNS^2 datasets, respectively. Rapid-CNS^2 datasets had the lowest scores among the tested datasets (Fig. 4c). We speculate that this is caused by the high number of missing values prevalent in these samples. Furthermore, we observed lower accuracies in the Heidelberg dataset than in the Nottingham dataset because of a higher share of samples run

https://doi.org/10.1038/s41591-025-03562-5

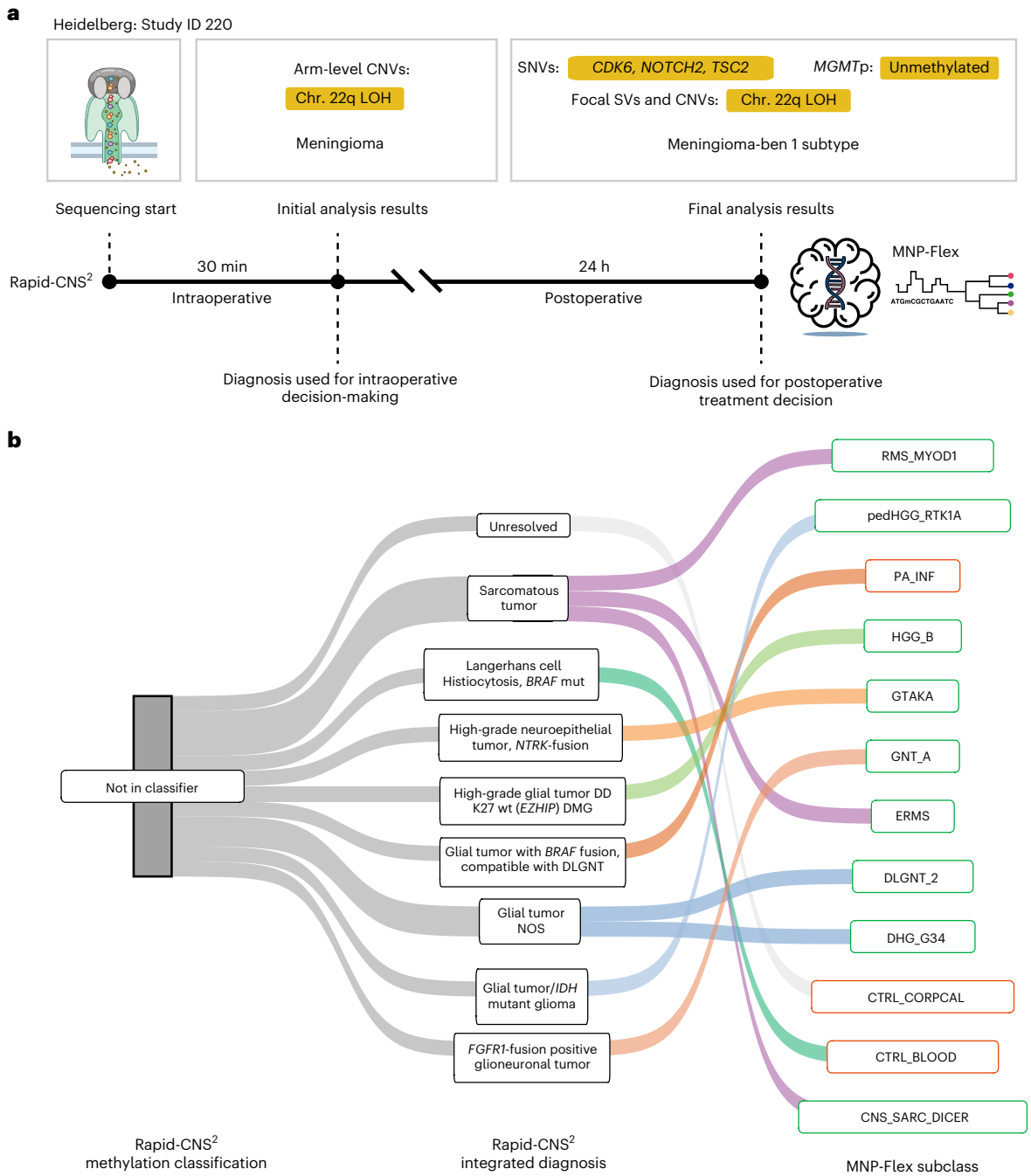

Fig. 6 | Integrated intraoperative and postoperative classification using Rapid-CNS² and MNP-Flex. a, Example of the end-to-end workflow combining intraoperative and postoperative analysis using Rapid-CNS² and methylation classification by MNP-Flex. **b**, For cases outside the scope of the Rapid-CNS² methylation classifier, additional layers of information like mutations, fusions and CNVs were used to provide an integrated diagnosis. Reclassification with MNP-Flex classified the cases as new entities only present in the MNP v.12 classifier. This resulted in accurate classifications for 9 of 12 cases (outlined in green). Two discrepant cases (outlined in orange) had low tumor content on histology inspection and were appropriately classified as 'control' classes. One diffuse leptomeningeal glioneuronal tumor (DLGNT) was predicted as pilocytic astrocytoma (outlined in orange), both of which are MAPK-activated low-grade glial and/or glioneuronal tumors. Credits: Nanopore schematic as well as signal and classification tree in the MNP-Flex logo in **a** was created using BioRender.com. Brain outline in **a** adapted from SVG Repo (https://www.svgrepo.com) under a Creative Commons license CC BY 4.0; DNA helix adapted from SVG Repo (https://www.svgrepo.com) under a Creative Commons license CC BY 4.0. DD, differential diagnosis; DMG, diffuse midline glioma; LOH, loss of heterozygosity; NOS, not otherwise specified; mut, mutation; wt, wild type.

with the older R9 flow cells, and on GridION or MinION instead of PromethION. Of note, Rapid-CNS² data generated with R10 already showed increased accuracy for MNP-Flex (Supplementary Fig. 9). Reassuringly, MNP-Flex reported lower calibrated scores over this dataset (Fig. 4b). As shown in Fig. 4b, most misclassifications occur in methylation families or with tumor microenvironment classes (Supplementary Fig. 8).

Collectively, we derived a cutoff of ≥0.7 for array samples and ≥0.3 for nonarray samples with MNP-Flex. We attained 99.6% accuracy (95% confidence intervals (CI) 99.6% to 99.7%) in identifying methylation families and 99.2% accuracy (95% CI 99.1% to 99.2%) for methylation subclasses on applying these thresholds across the comprehensive cohort (with MNP-RF ≥0.9 where applicable),

consisting of both frozen and FFPE samples, spanning five distinct technologies.

Intraoperative molecular classification

To test the shortest time to methylation classification and copy number calling, we retrospectively reanalyzed data from 36 representative samples from intraoperative frozen sections of the Heidelberg Rapid-CNS^2 dataset run on R9 flow cells. So far, these had been reported after, not during surgery. We sub-setted the data to reads generated at varying timepoints, enabling reconstruction of a real-world sequencing scenario. Twenty-nine of 35 (83%) samples with sufficient reads were assigned the correct methylation family from 15 min of sequencing (Fig. 5a). Within one hour of sequencing, 35 of 36 samples were accurately predicted. Importantly, concordant classifications consistently had significantly higher calibrated scores than discordant classifications. Short rejected reads from adaptive sampling result in uniform coverage over the genome leading to high-resolution copy number profiles in short periods. Arm-level alterations such as 1p, 7p and 22q loss were clearly resolved after 10 min of sequencing. Owing to CNV data, the single aberrant case could be identified as *IDH* wild-type glioblastoma on the basis of the diagnostic chromosome 7/10 alterations despite being predicted as methylation class 'high-grade *IDH*-mutant astrocytoma'. In addition, we simulated intraoperative setting for the 51 prospective samples (Supplementary Fig. 10), again demonstrating more precise classification. Finally, using a modified rapid library preparation protocol, we conducted actual real-time intraoperative sequencing on 18 samples in Heidelberg and Nottingham. Figure 5b demonstrates the predictions over 1 h of sequencing for two of these samples run at each center independently. Both were confidently predicted from 5 min of sequencing and results were forwarded to the surgeon in the operating room by phone to evaluate the entire procedure. Although these results are not yet used for surgical decision-making, a prospective study to assess the impact on outcome is being prepared. In alignment with our retrospective simulations, we found that integration of methylation and CNV data resulted in a more precise interpretation of 13 of 18 intraoperative samples within 30 min (Extended Data Figs. 3 and 4): seven samples of diffuse glioma could be identified as either *IDH*-mutant astrocytoma or *IDH* wild-type glioblastoma, which are impossible to distinguish on inspection of frozen section alone. Likewise, one ependymoma sample could be subtyped, yielding the high-risk supratentorial *ZFTA*-fusion positive group, as opposed to histologically indiscernible differential diagnoses of *YAP1*-fusion with lower risk profile. Five meningioma cases yielded insight into their copy number status, providing information associated with risk of recurrence. Only three cases were not substantially more informative than morphological inspection of the frozen section. Of note, one of these remained elusive after conventional testing as 'glial neoplasm'. In total, intraoperative Rapid-CNS^2 provided clinically relevant information on tumor (sub)type and risk profile in more than two-thirds (72.2%) of cases. Our intraoperative protocol yielded results on tumor classification and CNVs within 90 min of sample receipt, with sequencing and data interpretation constituting only 30 min or less, followed by comprehensive reporting with SNVs and/or Indels, gene fusions and fine-grained methylation classification on the next day.

Rapid-CNS^2 coupled with MNP-Flex improves diagnostic accuracy

Figure 6a demonstrates the end-to-end workflow combining Rapid-CNS^2 with MNP-Flex for Study ID 220. The sample was classified as a meningioma within 30 min of sequencing by the Rapid-CNS^2 methylation classifier. On completion of 24 h of sequencing, we detected SNVs in *CDK6*, *NOTCH2* and *TSC2*. In addition, we observed a homozygous deletion of chr. 22q and the *MGMT* promoter was unmethylated. MNP-Flex accurately predicted this sample to be the meningioma ben-1 subtype, a class not existing in the v.11 classifier versions (Supplementary Table 2). One intraoperative sample consistently achieved low scores for different classes over time even after 24 h of sequencing. MNP-Flex accurately diagnosed it as 'Diffuse pediatric-type high-grade glioma, RTK1, subclass A,' as corroborated by methylation array results obtained 40 days later (Extended Data Fig. 3). Moreover, of seven cases not unequivocally classifiable by Rapid-CNS^2 and five classifiable when leveraging all data, but not methylation alone in Rapid-CNS^2, eight were assigned a clear, correct methylation class and one a clear methylation family by MNP-Flex. Two of the remaining three samples were assigned 'control tissue' predictions, as confirmed by low tumor content using histology, and one was predicted as pilocytic astrocytoma but was otherwise diagnosed as diffuse leptomeningeal glioneuronal tumor, both MAPK-activated low-grade glial and/or glioneuronal tumors. Resolved samples could hence be unequivocally assigned an integrated diagnosis (Fig. 6b). This further demonstrates the value of granular subtyping using MNP-Flex and detailed molecular reporting with Rapid-CNS^2 over sole broad methylation classification with v.11-based models.

Discussion

Limitations associated with traditional comprehensive molecular diagnostics have long posed challenges for the field of neuropathology, resulting in a significant portion of the global population being denied access to vital diagnostic information. Rapid-CNS^2 combined with MNP-Flex—our platform-agnostic methylation classifier—enables reporting of an extensive array of molecular markers and fine-grained methylation classification in a variety of settings.

Nanopore sequencing has revolutionized the field of molecular research with handheld devices, easy library preparation, native nucleic acid sequencing resulting in long reads and base modification detection all at comparatively low costs[32,33]. Recent studies have demonstrated the potential of using shallow whole-genome nanopore sequencing to report methylation classification[11–15]. Rapid-CNS^2 supersedes these approaches to target clinically relevant genomic regions, while rejected reads provide sufficient breadth of coverage for methylation classification and fine copy number profiling[19]. Furthermore, intraoperative reporting of methylation classification and CNVs provides information crucial for surgical decisions. The approach offers the flexibility of analyzing a single sample or scaling up to 48 samples on the PromethION. Adaptive sampling only requires a text file that can be altered during a run, making the approach adaptable and readily transferable to other tumor indications. New adaptive sampling approaches like BOSS-RUNS now enable hands-free dynamic targeting[34]. Accumulation and investigation of long-read data have the potential to identify complex SVs as new molecular drivers missed by conventional short-read sequencing.

Owing to its accessible nature, actionable alterations reported by Rapid-CNS^2 will allow swift access to targeted therapies and molecularly informed disease management for patients in remote facilities as well. Although nanopore devices are certainly not yet widely available to neurosurgical groups, the fact that the capital expense for the smallest device allowing for Rapid-CNS^2 is of the magnitude of one-fiftieth of the minimal required set-up for conventional methylation testing will likely facilitate swift proliferation of the technology. Successful application of MNP-Flex to sequencing-based data from multiple sources across the world highlights its generalizability and potential utility in diverse settings. The static model of MNP-Flex compared with dynamic ad hoc classification in Rapid-CNS^2 enables it to cover the granularity of the MNP classifier v.12 at a much lower computational footprint than the broader ad hoc model. This has implications for the implementation of further iterations of the CNS or other methylation classification approaches, particularly for regulatory aspects, in which dynamic systems are viewed with much scrutiny. However, limitations to our approach must be acknowledged. A high prevalence of missing values and errors observed particularly in the Rapid-CNS^2 dataset, underscore the need for ongoing refinement of the model to address

such variability. Ultimately, the MNP-Flex model may replace the ad hoc model in the intraoperative setting, attenuating the variability associated with ad hoc approaches. Rapid-CNS^2 is currently limited to fresh or cryopreserved tissue because of the prevalence of short DNA fragments in paraffinized tissue posing challenges for effective computational targeting.

Rapid-CNS^2 utilizes single-molecule sequencing to identify genetic and epigenetic modifications on the same molecule. Integrated analysis of mutations, CNVs and methylation—especially with long reads—holds promise for detecting subclonal reads accurately[33,35,36]. Subclonal methylation classes could be identified by a robust MNP-Flex model providing insights for potential heterogeneity-informed targeted therapies. Anticipated advancements in nanopore technology, clonotyping and methylation classification models suggest a future in which disease monitoring via noninvasive liquid biopsy becomes routine[37,38]. This approach could identify clonal diversity through methylation classification, target emerging clones therapeutically and assess treatment efficacy by estimating tumor burden[38–40].

The current release of Rapid-CNS^2 and MNP-Flex provides the basis for making these advancements and further updates of molecular classification guidelines more equally accessible and readily available on a global scale.

Online content

Any methods, additional references, Nature Portfolio reporting summaries, source data, extended data, supplementary information, acknowledgements, peer review information; details of author contributions and competing interests; and statements of data and code availability are available at https://doi.org/10.1038/s41591-025-03562-5.

References

1. Platten, M. et al. A vaccine targeting mutant IDH1 in newly diagnosed glioma. *Nature* **592**, 463–468 (2021).
2. Grassl, N. et al. A H3K27M-targeted vaccine in adults with diffuse midline glioma. *Nat. Med.* **29**, 2586–2592 (2023).
3. Bouffet, E. et al. Dabrafenib plus trametinib in pediatric glioma with BRAF V600 mutations. *N. Engl. J. Med.* **389**, 1108–1120 (2023).
4. Hargrave, D. R. et al. Phase II trial of dabrafenib plus trametinib in relapsed/refractory BRAF V600-mutant pediatric high-grade glioma. *J. Clin. Oncol.* **41**, 5174–5183 (2023).
5. Capper, D. et al. DNA methylation-based classification of central nervous system tumours. *Nature* **555**, 469–474 (2018).
6. Sturm, D. et al. Multiomic neuropathology improves diagnostic accuracy in pediatric neuro-oncology. *Nat. Med.* **29**, 917–926 (2023).
7. Louis, D. N. et al. The 2021 WHO Classification of Tumors of the Central Nervous System: a summary. *Neuro Oncol.* **23**, 1231–1251 (2021).
8. Sahm, F. et al. Molecular diagnostic tools for the World Health Organization (WHO) 2021 classification of gliomas, glioneuronal and neuronal tumors; an EANO guideline. *Neuro Oncol.* **25**, 1731–1749 (2023).
9. Horbinski, C. et al. NCCN Guidelines® Insights: Central Nervous System Cancers, Version 2.2022. *J. Natl Compr. Canc. Netw.* **21**, 12–20 (2023).
10. Buckland, M. E. et al. Announcing the Asian Oceanian Society of Neuropathology guidelines for Adapting Diagnostic Approaches for Practical Taxonomy in Resource-Restrained Regions (AOSNP-ADAPTR). *Brain Pathol.* **34**, e13201 (2023).
11. Afflerbach, A. K. et al. Classification of brain tumors by nanopore sequencing of cell-free DNA from cerebrospinal fluid. *Clin. Chem.* **70**, 250–260 (2024).
12. Vermeulen, C. et al. Ultra-fast deep-learned CNS tumour classification during surgery. *Nature* **622**, 842–849 (2023).
13. Simon, M. et al. Rapid DNA methylation-based classification of pediatric brain tumours from ultrasonic aspirate specimens. *J. Neurooncol.* **169**, 73–83 (2024).
14. Djirackor, L. et al. Intraoperative DNA methylation classification of brain tumors impacts neurosurgical strategy. *Neurooncol. Adv.* **3**, vdab149 (2021).
15. Kuschel, L. P. et al. Robust methylation-based classification of brain tumours using nanopore sequencing. *Neuropathol. Appl. Neurobiol.* **49**, e12856 (2023).
16. Euskirchen, P. et al. Same-day genomic and epigenomic diagnosis of brain tumors using real-time nanopore sequencing. *Acta Neuropathol.* **134**, 691–703 (2017).
17. Loose, M. et al. Real-time selective sequencing using nanopore technology. *Nat. Methods* **13**, 751–754 (2016).
18. Payne, A. et al. Readfish enables targeted nanopore sequencing of gigabase-sized genomes. *Nat. Biotechnol.* **39**, 442–450 (2021).
19. Patel, A. et al. Rapid-CNS2: rapid comprehensive adaptive nanopore-sequencing of CNS tumors, a proof-of-concept study. *Acta Neuropathol.* **143**, 609–612 (2022).
20. Zhao, S., Agafonov, O., Azab, A., Stokowy, T. & Hovig, E. Accuracy and efficiency of germline variant calling pipelines for human genome data. *Sci. Rep.* **10**, 20222 (2020).
21. Bady, P. et al. MGMT methylation analysis of glioblastoma on the Infinium methylation BeadChip identifies two distinct CpG regions associated with gene silencing and outcome, yielding a prediction model for comparisons across datasets, tumor grades, and CIMP-status. *Acta Neuropathol.* **124**, 547–560 (2012).
22. Braczynski, A. K. et al. High density DNA methylation array is a reliable alternative for PCR-based analysis of the MGMT promoter methylation status in glioblastoma. *Pathol. Res. Pract.* **216**, 152728 (2020).
23. Halldorsson, S. et al. Accurate and comprehensive evaluation of O6-methylguanine-DNA methyltransferase promoter methylation by nanopore sequencing. *Neuropathol. Appl. Neurobiol.* **50**, e12984 (2024).
24. Jones, D. T. W. et al. Tandem duplication producing a novel oncogenic BRAF fusion gene defines the majority of pilocytic astrocytomas. *Cancer Res.* **68**, 8673–8677 (2008).
25. Gan, H. K., Cvrljevic, A. N. & Johns, T. G. The epidermal growth factor receptor variant III (EGFRvIII): where wild things are altered. *FEBS J.* **280**, 5350–5370 (2013).
26. Singh, O. EPCO-26. Intratumoral heterogeneity of GBM identified and characterized by a multisampling approach and methylation profiling. *Neuro-Oncology* **25**, v129 (2023).
27. Wenger, A. et al. Intratumor DNA methylation heterogeneity in glioblastoma: implications for DNA methylation-based classification. *Neuro Oncol.* **21**, 616–627 (2019).
28. Priesterbach-Ackley, L. P. et al. Brain tumour diagnostics using a DNA methylation-based classifier as a diagnostic support tool. *Neuropathol. Appl. Neurobiol.* **46**, 478–492 (2020).
29. Friedman, J. H. Greedy function approximation: a gradient boosting machine. *Ann. Stat.* **29**, 1189–1232 (2001).
30. Capper, D. et al. Practical implementation of DNA methylation and copy-number-based CNS tumor diagnostics: the Heidelberg experience. *Acta Neuropathol.* **136**, 181–210 (2018).
31. Wu, Z. et al. Impact of the methylation classifier and ancillary methods on CNS tumor diagnostics. *Neuro Oncol.* **24**, 571–581 (2022).
32. Wang, Y. et al. Nanopore sequencing technology, bioinformatics and applications. *Nat. Biotechnol.* **39**, 1348–1365 (2021).
33. Kolmogorov, M. et al. Scalable nanopore sequencing of human genomes provides a comprehensive view of haplotype-resolved variation and methylation. *Nat. Methods* **20**, 1483–1492 (2023).
34. Weilguny, L. et al. Dynamic, adaptive sampling during nanopore sequencing using Bayesian experimental design. *Nat. Biotechnol.* **41**, 1018–1025 (2023).

35. Fu, Y. et al. MethPhaser: methylation-based haplotype phasing of human genomes. *Nat. Commun.* **15**, 5327 (2024).
36. Watkins, T. B. K. et al. Refphase: multi-sample phasing reveals haplotype-specific copy number heterogeneity. *PLoS Comput. Biol.* **19**, e1011379 (2023).
37. Bailey, C. et al. Tracking cancer evolution through the disease course. *Cancer Discov.* **11**, 916–932 (2021).
38. Abbosh, C. et al. Tracking early lung cancer metastatic dissemination in TRACERx using ctDNA. *Nature* **616**, 553–562 (2023).
39. Black, J. R. M., McGranahan, N., Black, J. R. M. & McGranahan, N. Genetic and non-genetic clonal diversity in cancer evolution. *Nat. Rev. Cancer* **21**, 379–392 (2021).
40. Baca, S. C. et al. Liquid biopsy epigenomic profiling for cancer subtyping. *Nat. Med.* **29**, 2737–2741 (2023).

Areeba Patel[1,2,3], Kirsten Göbel[1,2], Sebastian Ille[4], Felix Hinz[1,2], Natalie Schoebe[1,2], Henri Bogumil[1,2], Jochen Meyer[1,2], Michelle Brehm[1,2], Helin Kardo[1,2], Daniel Schrimpf[1,2], Artem Lomakin[5], Michael Ritter[1,2], Pauline Göller[1,2], Paul Kerbs[1,2], Lisa Pfeifer[1,2], Stefan Hamelmann[1,2], Christina Blume[1,2], Franziska M. Ippen[1,2,6,7], Natalie Berghaus[1,2], Philipp Euskirchen[8,9], Leonille Schweizer[10,11,12], Claus Hultschig[13], Nadine Van Roy[14], Jo Van Dorpe[15], Joni Van der Meulen[14], Siebe Loontiens[14], Franceska Dedeurwaerdere[16], Henning Leske[17,18], Skarphéðinn Halldórsson[17], Graeme Fox[19], Simon Deacon[20,21], Inswasti Cahyani[19], Nadine Holmes[19], Satrio Wibowo[19], Rory Munro[19], Dan Martin[20,21], Abid Sharif[20,21], Mark Housley[20,21], Robert Goldspring[20,21], Sebastian Brandner[22,23], Somak Roy[24], Jürgen Hench[13], Stephan Frank[13], Andreas Unterberg[4], Violaine Goidts[25], Natalie Jäger[3,26], Simon Paine[20,21], Stuart Smith[20,21], Christel Herold-Mende[4], Wolfgang Wick[6,27], Stefan M. Pfister[3,7,26,28], Einar O. Vik-Mo[17,29], Andreas von Deimling[1,2], Sandro Krieg[4], David TW Jones[3,30], Matthew Loose[19], Matthias Schlesner[31], Martin Sill[3,26,32] ✉ & Felix Sahm[1,2,3,32] ✉

[1]Department of Neuropathology, University Hospital Heidelberg, Heidelberg, Germany. [2]Clinical Cooperation Unit Neuropathology, German Consortium for Translational Cancer Research (DKTK), German Cancer Research Center (DKFZ), Heidelberg, Germany. [3]Hopp Children's Tumor Center (KiTZ), Heidelberg, Germany. [4]Department of Neurosurgery, Heidelberg University Hospital, Heidelberg, Germany. [5]Division of Artificial Intelligence in Oncology, German Cancer Research Center (DKFZ), Heidelberg, Germany. [6]Department of Neurology, University Hospital Heidelberg, Heidelberg, Germany. [7]National Center for Tumor Diseases (NCT), Heidelberg, Germany. [8]Department of Neuropathology, Charité–Universitätsmedizin Berlin, corporate member of Freie Universität Berlin and Humboldt Universität zu Berlin, Berlin, Germany. [9]German Cancer Consortium (DKTK), partner site Berlin, German Cancer Research Center (DKFZ), Heidelberg, Germany. [10]Institute of Neurology (Edinger Institute), University Hospital Frankfurt, Goethe University, Frankfurt am Main, Germany. [11]Frankfurt Cancer Institute (FCI), Frankfurt am Main, Germany. [12]German Cancer Consortium (DKTK), Partner Site Frankfurt/Mainz, German Cancer Research Center (DKFZ), Heidelberg, Germany. [13]Institute for Pathology, Division of Neuropathology, University Hospital Basel, Basel, Switzerland. [14]Center for Medical Genetics Ghent, Ghent University Hospital, Ghent University, Ghent, Belgium. [15]Department of Pathology, Ghent University Hospital, Ghent University, Ghent, Belgium. [16]Department of Pathology, AZ Delta, Roeselare, Belgium. [17]Vilhelm Magnus Laboratory, Department of Neurosurgery, Oslo University Hospital, Oslo, Norway. [18]Department of Pathology, Oslo University Hospital, Oslo, Norway. [19]School of Life Sciences, University of Nottingham, Nottingham, UK. [20]School of Medicine, University of Nottingham, Nottingham, UK. [21]Nottingham University Hospitals NHS Trust, Nottingham, UK. [22]Division of Neuropathology, National Hospital for Neurology and Neurosurgery, University College London Hospitals NHS Foundation Trust, London, UK. [23]Department of Neurodegenerative Disease, University College London, Institute of Neurology, London, UK. [24]Cincinnati Children's Hospital Medical Center, Cincinnati, OH, USA. [25]Brain Tumor Translational Targets, German Cancer Research Center (DKFZ), Heidelberg, Germany. [26]Division of Pediatric Neurooncology, German Cancer Research Center (DKFZ) and German Cancer Consortium (DKTK), Heidelberg, Germany. [27]Clinical Cooperation Unit Neurooncology, German Cancer Consortium within German Cancer Research Center, Heidelberg, Germany. [28]Department of Pediatric Hematology and Oncology, Heidelberg University Hospital, Heidelberg, Germany. [29]Institute for Clinical Medicine, University of Oslo, Oslo, Norway. [30]Division of Pediatric Glioma Research, German Cancer Research Center (DKFZ), Heidelberg, Germany. [31]Biomedical Informatics, Data Mining and Data Analytics, University of Augsburg, Augsburg, Germany. [32]These authors contributed equally: Martin Sill, Felix Sahm.
✉e-mail: m.sill@kitz-heidelberg.de; felix.sahm@med.uni-heidelberg.de

Methods

Ethics and inclusion statement

This study complied with ethics regulations as approved by the Ethics Committee Heidelberg (S-318/2022), Ethics Committee Nottingham (11/EM/0076) and Ethical Committee, Ghent University Hospital (Clinical Trial Number/IRB B6702021000850). Informed consent was obtained for all patients and patients were not compensated for participation. Patient samples were included if they presented with a suspected CNS tumor and had undergone surgery to ensure tissue availability. Patient sex was self-reported and available for 239 patients in the Rapid-CNS[2] cohort. Age, sex and/or gender were not included in the study design, because the focus was on validating a platform for molecular profiling. Based on available literature, such profiling accuracy is not known to be influenced by age, sex or gender. No exclusions were made based on race, ethnicity, sex, age, gender or other social factor.

Tissue

For Rapid-CNS[2], we required a minimum of 5 mg of fresh or cryopreserved tissue. We recommend 2.5 µg of starting DNA for the best results, but we were able to successfully perform sequencing with 800 ng of starting DNA on the P2 Solo. All results presented in this study were generated for research purposes only and were not used to influence clinical or surgical decisions.

Rapid-CNS[2]

DNA was extracted using the Maxwell RSC Blood DNA Kit (Promega, cat. no. AS1400) following the manufacturer's instructions. In summary, 40 × 10 µm of fresh-frozen tumor tissue was incubated with 400 µl of lysis buffer and 40 µl of proteinase K, at 56 °C overnight, with continuous agitation at 550 rpm. The following day, samples were transferred to well 1 of a Maxwell cartridge. DNA extraction was performed using the recommended protocol on the device. For sequencing performed in Heidelberg, two protocols were followed depending on the flow cells used. For R9 flow cells, we used the previously described protocol[19]. The following describes the protocol for R10 flow cells: 2.5 µg of extracted DNA was sheared into 10-kb fragments in 60 µl of nuclease-free water using a Covaris g-Tube (Covaris, cat. no. 520079) following the manufacturer's instructions. A sequencing library was prepared using the Ligation Sequencing Kit (Oxford Nanopore Technologies (ONT), cat. no. SQK-LSK114) and the NEBNext Companion Module (New England Biolabs, cat. no. E7180S) with only minor adjustments to the original protocol (ONT, Ligation Sequencing DNA V14 (SQK-LSK114)). In brief, DNA repair and end-prep was carried out starting with 58 µl of sheared DNA as input. The ratio of AMPure beads for bead clean-up was adjusted to the volume of the sheared DNA, as proposed in ref. 33. Adapter ligation and bead clean-up were performed using the short fragment buffer. DNA was eluted in 15 µl for a MinION sequencing run, and in 25 µl for a PromethION sequencing run. If sequencing was performed with a MinION (FLO-MIN114, R10) flow cell, flow cells were primed using the BSA supplement and sequenced using a GridION X5. If sequencing was performed with a PromethION (FLO-PRO114M, R10) flow cell, flow cells were primed without BSA supplement and sequenced on the P2 Solo. Sequencing on both devices was performed with 600–700 ng of DNA library for 24 h with all available channels in adaptive sampling mode, using the hg19 genome build as a reference file and a custom.bed file for panel B as described previously for target enrichment[19].

Rapid-CNS[2] analysis

We iteratively refined the Rapid-CNS[2] pipeline to keep pace with evolving developments and tools. In its initial version, Rapid-CNS[2] v.1 incorporated guppy v.4.4.0 base-calling, alignment and megalodon (https://github.com/nanoporetech/megalodon) methylation calling as described previously[19]. Subsequent improvements in Rapid-CNS[2] integrated guppy v.5 onwards, enabling simultaneous base-calling, methylation calling using remora (https://github.com/nanoporetech/remora) and alignment in a single step. We developed both bash and Nextflow pipelines to ensure adaptability across diverse environments. At Heidelberg, we ran two versions depending on the infrastructure—local or load sharing facility. We deployed the pipeline in multi-GPU (graphical processing unit) mode on the load sharing facility cluster with a primarily conda-based workflow. For the local deployment, we used a single NVIDIA RTX 3090 Ti GPU powered local workstation with a Dockerised pipeline. We performed base-calling in a base-call server-supervisor mode for ONT's proprietary software guppy or Dorado (https://github.com/nanoporetech/dorado) as specified in Supplementary Table 1. For the multi-GPU mode, we used 15 base-call clients for a 3 GPU setting with available NVIDIA GPU models (RTX 2080 Ti, A100, V100). For a single GPU, we ran guppy_basecall_supervisor or subsequently ont_basecall_supervisor with five clients. The super accuracy model with 5-mC detection was used for base-calling for all samples.

Because we evaluated each sample at the time of receipt, versions of the tools used for the respective libraries are indicated in Supplementary Table 1. We aligned reads to the hg19 reference genome using guppy or Dorado. Methylation values were extracted using modbam2bed (https://github.com/epi2me-labs/modbam2bed, v.0.5.3) with the --cpg parameter. We performed liftover of the methylation bed files to the hg38 genome using the liftOver tool[41]. *MGMT* promoter status was calculated using a logistic regression-based binomial classifier as previously described if the sample had minimum 3× coverage over the region spanning chr10:129466536–129467536. Methylation classification was performed by retraining sample-specific ad hoc random forest models[19]. We performed SNV detection and filtering using PEPPER-Margin-DeepVariant (r0.4 for R9 flow cells and r0.8 for R10 flow cells) on the reads mapping to the targeted regions[42]. The subset bam file was generated using the bedtools (v.2.30.0) intersect function[43]. The analysis was conducted with a minimum base quality score of 7, a maximum read depth of 8,000 and nanopore-specific adjustments (-X ont). We extracted read depth, allelic depth for forward strand and allelic depth for reverse strand from on-target bam files. This was followed by bcftools view to generate variant call format outputs. SNVs were annotated using ANNOVAR (downloaded 7 May 2021) and filtered for clinical relevance using a custom script[44]. We called CNVs on the entire bam file with a bin size of 100 kb using default parameters for CNVpytor (v.1.2.1 for R9 flow cells and v.1.3.1 for R10 flow cells)[45]. The copy number status of relevant genes was reported using a custom python script. The script parses the pytor file obtained as output of CNVpytor. If the complete gene was covered by the bin, the copy number status of the bin was assigned to the gene. SV detection used Sniffles2 (v.2.2) in nongermline mode, followed by annotation using AnnotSV (v.3.0.7)[46,47]. Visualization of methylation values in the *MGMT* promoter region was carried out using methylartist (v.1.2.8)[48]. Bam files and variant call formats were visualized in the integrated genome viewer. An updated Nextflow pipeline compatible with latest version tools, as available in August 2024, is also made available. In this pipeline, GPU-supported variant calling is performed using Clara Parabricks[49].

The pipelines are available on GitHub. The bash pipeline that was used to analyze samples is https://github.com/areebapatel/Rapid-CNS2_sh and the updated Nextflow workflow is https://github.com/areebapatel/Rapid-CNS2_nf.

Protocol for Nottingham

For the archival samples, we ran adaptive sampling using GridION with three loads per patient using the Ligation Sequencing Kit on R10.4.1 flow cells. For the diagnostic cases, we ran adaptive sampling using readfish (https://github.com/LooseLab/readfish) on a P2 Solo for 24 h for each sample using R10.4.1 flow cells and a rapid based kit[18,50]. For the purposes of this manuscript, samples were analyzed at the end of 72 h (archival) or 24 h (diagnostic) using a Nextflow pipeline based on

the Rapid-CNS[2] protocol. We replaced the DeepVariant step with the ONT wf-human-variation pipeline (https://github.com/epi2me-labs/wf-human-variation).

Intraoperative protocol

For the intraoperative protocol, we require a minimum of 5 mg of tissue. In Nottingham, we prepared samples with the ONT Ultra-Long DNA Sequencing Kit using an adjusted protocol (SQK-ULK114) (https://protocols.io/view/intra-operative-nanopore-sequencing-to-classify-brc65qzg5w). For intraoperative samples sequenced in Heidelberg, we performed protein cracking using Maxwell DNA extraction with a PreCellys cell/tissue homogenization device instead of shearing by needle. We analyzed samples in real-time using the ROBIN pipeline at Nottingham and a custom pipeline at Heidelberg[51]. Briefly, the pipelines base-call and align the fast5 and/or pod5 files using Dorado (dna_r10.4.1_e8.2_400bps_modbases_5mc_cg_hac_prom) as soon they are written to the output folder. Methylation values were extracted using modbam2bed (Heidelberg) and modkit (Nottingham), respectively. We ran the Rapid-CNS[2] methylation classifier on the files upon generation. We ran QDNAseq for copy number variant calling on bam files at 5-min intervals.

Nanopore whole-genome sequencing

Genomic DNA was extracted from fresh or fresh-frozen tumor biopsies with the Qiagen Blood & Tissue Mini Kit. Briefly, 10–30 mg of tissue were homogenized in ATL buffer in a TissueLyser bead mill at 30 Hz for 30 s, followed by digestion with proteinase K for 3–16 h. Buffer AL and RNAse were added to the sample and incubated at room temperature for 5 min, followed by incubation at 70 °C for 10 min. EtOH (100%) was added to the sample before washing and elution on spin columns. DNA purity was evaluated with NanoDrop (260/230 > 1.8 and 260/280 > 1.9 was deemed sufficient) and concentration was measured using a Qubit DNA broad-range kit. Between 1 and 3 µg of gDNA were used as input for sequencing library preparation with Ligation Sequencing Kit V14 (SQK-LSK114) according to the manufacturer's protocol (Ligation Sequencing DNA V14). Then 300 ng of DNA library was loaded onto PromethION flow cells (FLO-PRO114M) on a P24 sequencing device, one library per flow cell, and sequenced for 80 h. Flow cells were washed and reloaded if necessary after 24 or 48 h of sequencing (Flow Cell Wash Kit; ONT, cat. no. EXP-WSH004). Live base-calling, methylation calling and mapping (hg38) were performed using MinKNOW software (v.23.07) with Dorado (v.7.1.14). Base-calling was performed with the super-high accuracy model (dna_r10.4.1_e8.2_400bps_sup@v4.1.0), sequences below the quality threshold of 10 were excluded from further analysis. Per-site methylation extraction and across-strand aggregation from modified.bam files was performed in the epi2me-labs suite through the wf-human-variation (v.1.8.1) workflow with modkit (v.0.2.0) or modbam2bed (v.0.10.0). Whole-genome methylation.bed files were cross-referenced with EPIC probe genomic locations with the bedtools intersect function.

Twist panel sequencing

DNA was extracted from FFPE tissue. Two hundred nanograms of DNA was used as input for the Twist Human Methylome Panel. The protocol provided by the Twist Targeted Methylation Sequencing Protocol was followed[52]. The libraries were sequenced on an Illumina NovaSeq 6000 using paired-end 150 bp reads (2 × 150 bp). Methylation values were extracted using a Nextflow pipeline (https://nf-co.re/methylseq/1.6.1).

WGBS Heidelberg

Samples were prepared for the WGBS library using the 'Swift Accel-NGS Methyl-Seq DNA' kit and sequenced on the Illumina HiSeq X Ten v.2.5 in paired-end mode, with one lane per tumor sample, resulting in an average genome coverage of ~30X per sample. WGBS sequencing data were analyzed using methylCtools (https://github.com/hovestadt/methylCtools) as part of the Omics IT and Data Management Core Facility Bisulfite core workflow (https://github.com/DKFZ-ODCF/AlignmentAndQCWorkflows; AlignmentAndQCWorkflows:1.2.73-2)[53,54]. In brief, methylCtools builds upon BWA and adds functionality for aligning bisulfite-treated DNA to a reference genome in a similar manner to that described previously[54]. Sequencing reads were adapter-trimmed and translated to a fully C-to-T converted state. Alignments were performed against a single index of both in silico bisulfite-converted strands of the human reference genome (hs37d5 including PhiX) using BWA. Previously translated bases were translated back to their original state, and reads mapping antisense to the respective reference strand were removed. Single-base-pair methylation ratios (β values) were determined by quantifying evidence for methylated (unconverted) and unmethylated (converted) cytosines at all CpG positions. Only properly paired or singleton reads with mapping quality of ≥1 and bases with a Phred-scaled quality score of ≥20 were considered. We used processed WGBS data from the publicly available PBCA-DE cohort on the International Cancer Genome Consortium portal.

NGS panel sequencing and EPIC array analysis

Nucleic acid extraction, NGS panel sequencing, NGS RNA sequencing and DNA methylation array data were produced and analyzed as previously described[19,30,55,56]. At the Department of Neuropathology, University Hospital Heidelberg, DNA sequencing was performed using a customized enrichment and hybrid capture-based NGS gene panel, covering the entire coding regions (all exons ±25 bp) and selected intronic and promoter regions of 130 genes. This panel was designed to detect SNVs, small Indels, exonic rearrangements and recurrent fusion events. RNA sequencing was performed for selected samples based on indications of fusion events from targeted DNA sequencing or copy number data derived from methylation arrays, assignment to DNA methylation classes associated with fusion events or where RNA sequencing was expected to provide additional diagnostic insights. DNA methylation data obtained using the Illumina Infinium HumanMethylation450 and MethylationEPIC v.1 BeadChip arrays was classified using the MNP v.11b4 and MNP v.12.8 classifiers, while that obtained using the MethylationEPIC v.2 BeadChip arrays were classified only using the v.12.8 classifier (https://www.molecularneuropathology.org/mnp/).

Time to classification analysis

For 39 Rapid-CNS[2] samples sequenced in Heidelberg, we conducted simultaneous base-calling and alignment to the hg19 genome using guppy 6.4.6 with the super accuracy configuration and 5-mC modification detection. Sequencing summary files aided in extracting cumulative reads at time intervals (5, 10, … 1,440 min). Methylation values were extracted using modbam2bed (https://github.com/epi2me-labs/modbam2bed), liftover to hg38 genome was performed and the ad hoc Rapid-CNS[2] classifier was applied[19]. Simultaneously, CNV calling was performed using QDNAseq (v.1.32.0) with a bin size of 1 Mb (ref. 57).

MNP-Flex

The MNP-Flex classification model was trained by applying gradient-boosted decision trees using the popular xgboost algorithm (R package xgboost 2.01)[58]. The MNP v.12 training dataset which includes 7,495 samples comprising 184 methylation classes, described in detail on our website (https://www.molecularneuropathology.org), was split into training and validation data with a 70% and 30% data split (R package caret 6.0-94), respectively. Raw signal intensities were obtained from IDAT files using the minfi Bioconductor package v.1.21.4 (ref. 59). Illumina EPIC samples and 450K samples were merged to a combined dataset by selecting the intersection of probes present on both arrays (combineArrays function, minfi). Each sample was individually normalized by performing a background correction (shifting of the 5% percentile of negative control probe intensities to 0)

and a dye-bias correction (scaling of the mean of normalization control probe intensities to 10,000) for both color channels. Subsequently, a correction for the type of material tissue (FFPE or frozen) and array type (450K or EPIC) was performed by fitting univariable, linear models to the $\log_2$-transformed intensity values (removeBatchEffect function, limma package v.3.30.11). The methylated and unmethylated signals were corrected individually. Beta-values were calculated from the retransformed intensities using an offset of 100 (as recommended by Illumina). For CpG probe filtering, probes valid according to the filtering criteria in ref. 60 were selected (https://zwdzwd.github.io/InfiniumAnnotation), resulting in 357,521 probes after additionally removing probes located on the X and Y chromosomes. The CpG probes have been further filtered to the 100K probes showing highest standard deviation. To be able to later perform model inference on other potential low coverage sequencing-based data sources, the training data has been binarized by applying a threshold of >0.6 to the preprocessed beta methylation values.

Finally, the model was trained with 'mulitclass:softprob' as objective function for 2,306 iterations with a learning rate of eta = 0.01 until the early stopping was triggered, achieving a multiclass logloss of 0.1969 on the validation data.

Concordance analysis

For Rapid-CNS^2, our concordance analysis focused on panel regions in both NGS and Rapid-CNS^2 bam files. 'SNVs recovered' represented the percentage of variants identified in NGS data that were also present in Rapid-CNS^2 variant calls. We compared CNV profiles with their corresponding methylation array-based profiles by visual inspection. *MGMT* promoter methylation status was compared with the predictions for the methylation array data using Bady's method[21]. Samples with a coverage <3× over the *MGMT* region were deemed 'unclassifiable'. Only clinically relevant fusions were compared with corresponding data from NGS RNA sequencing. We compared methylation classes with their corresponding MNP v.11 prediction for the methylation array. Because v.11 is unavailable for samples profiled using EPIC v.2 chips, we compared those with an 'inferred' class from the MNP v.12 prediction. Integrated diagnoses were made by neuropathologists in a 'real-world' setting. 'Conventional' integrated diagnoses were issued by considering histopathology, clinical data and molecular analysis results from the NGS + Infinium Methylation array. Rapid-CNS^2 integrated diagnoses were similarly issued using molecular results from Rapid-CNS^2 instead.

For MNP-Flex, data from all validation samples were subset to sites present in the Illumina Infinium MethylationEPIC array and the *MGMT* promoter region. For methylation array data, we compared subclass and family-level predictions with the corresponding MNP-RF predictions. For nonmethylation array samples, we calculated concordance for MNP-Flex samples based on predictions made for corresponding MethylationEPIC array profiles by MNP-RF or available neuropathology data assessment (Supplementary Table 2). CI values were calculated using the binom R package. Plots were generated using ggplot2 (v.3.5.1), ggsankey (v.0.0.99999), ggridges (v.0.5.4), patchwork (v.1.1.3) and related R packages for visualization. The MNP-Flex scores obtained from analyzing samples gathered from FFPE and frozen sources were tested with a nonparametric equivalence test available through the R package TOSTER (v.0.8.3) using an upper and lower equivalence bound of 0.01.

Reporting summary

Further information on research design is available in the Nature Portfolio Reporting Summary linked to this article.

Data availability

Data generated in this study are available via Zenodo at https://doi.org/10.5281/zenodo.13351527 (ref. 61). Deidentified sequencing data will be made available for academic research use only upon request to F.S. (felix.sahm@med.uni-heidelberg.de). Requests will be reviewed and responded to within 14 working days. Source data are provided with this paper.

Code availability

Analysis code for different use cases of Rapid-CNS^2 and preprocessing code to convert bedmethyl files to MNP-Flex compatible input is available via GitHub at https://github.com/areebapatel/Rapid-CNS2_sh and https://github.com/areebapatel/Rapid-CNS2_nf.

References

41. Hinrichs, A. S. et al. The UCSC Genome Browser Database: update 2006. *Nucleic Acids Res.* **34**, D590-8 (2006).
42. Shafin, K. et al. Haplotype-aware variant calling with PEPPER-Margin-DeepVariant enables high accuracy in nanopore long-reads. *Nat. Methods* **18**, 1322–1332 (2021).
43. Quinlan, A. R. & Hall, I. M. BEDTools: a flexible suite of utilities for comparing genomic features. *Bioinformatics* **26**, 841–842 (2010).
44. Wang, K., Li, M. & Hakonarson, H. ANNOVAR: functional annotation of genetic variants from high-throughput sequencing data. *Nucleic Acids Res.* **38**, e164 (2010).
45. Suvakov, M., Panda, A., Diesh, C., Holmes, I. & Abyzov, A. CNVpytor: a tool for copy number variation detection and analysis from read depth and allele imbalance in whole-genome sequencing. *Gigascience* **10**, giab074 (2021).
46. Smolka, M. et al. Detection of mosaic and population-level structural variants with Sniffles2. *Nat. Biotechnol.* **42**, 1571–1580 (2024).
47. Geoffroy, V. et al. The AnnotSV webserver in 2023: updated visualization and ranking. *Nucleic Acids Res.* **51**, W39–W45 (2023).
48. Cheetham, S. W., Kindlova, M. & Ewing, A. D. Methylartist: tools for visualizing modified bases from nanopore sequence data. *Bioinformatics* **38**, 3109–3112 (2022).
49. O'Connell, K. A. et al. Accelerating genomic workflows using NVIDIA Parabricks. *BMC Bioinformatics* **24**, 221 (2023).
50. Munro, R. et al. Enhancing nanopore adaptive sampling for PromethION using readfish at scale. *Genome Res.* https://doi.org/10.1101/gr.279329.124 (2025).
51. Deacon, S. et al. ROBIN: a unified nanopore-based sequencing assay integrating real-time, intraoperative methylome classification and next-day comprehensive molecular brain tumour profiling for ultra-rapid tumour diagnostics. Preprint at *medRxiv* https://doi.org/10.1101/2024.09.10.24313398 (2024).
52. Vaisvila, R. et al. Enzymatic methyl sequencing detects DNA methylation at single-base resolution from picograms of DNA. *Genome Res.* **31**, 1280–1289 (2021).
53. Reisinger, E. et al. OTP: an automatized system for managing and processing NGS data. *J. Biotechnol.* **261**, 53–62 (2017).
54. Hovestadt, V. et al. Decoding the regulatory landscape of medulloblastoma using DNA methylation sequencing. *Nature* **510**, 537–541 (2014).
55. Stichel, D. et al. Routine RNA sequencing of formalin-fixed paraffin-embedded specimens in neuropathology diagnostics identifies diagnostically and therapeutically relevant gene fusions. *Acta Neuropathol.* **138**, 827–835 (2019).
56. Sahm, F. et al. Next-generation sequencing in routine brain tumor diagnostics enables an integrated diagnosis and identifies actionable targets. *Acta Neuropathol.* **131**, 903–910 (2015).
57. Scheinin, I. et al. DNA copy number analysis of fresh and formalin-fixed specimens by shallow whole-genome sequencing with identification and exclusion of problematic regions in the genome assembly. *Genome Res.* **24**, 2022–2032 (2014).

58. Chen, T. & Guestrin, C. *Proc. 22nd ACM SIGKDD International Conference on Knowledge Discovery and Data Mining* (Association for Computing Machinery, 2016).
59. Aryee, M. J. et al. Minfi: a flexible and comprehensive Bioconductor package for the analysis of Infinium DNA methylation microarrays. *Bioinformatics* **30**, 1363–1369 (2014).
60. Zhou, W., Laird, P. W. & Shen, H. Comprehensive characterization, annotation and innovative use of Infinium DNA methylation BeadChip probes. *Nucleic Acids Res.* **45**, e22 (2017).
61. Patel, A. & Sill, M. Data for Rapid-CNS^2 and MNP-Flex. *Zenodo* https://doi.org/10.5281/zenodo.13351526 (2024).

Acknowledgements

This work was supported by the Schwiete-Foundation Mannheim via a grant to F.S., the DFG via SFB1389 to V.G., C.H.-M., S.M.P., M. Schlesner, D.T.W.J., W.W., A.v.D. and F.S., and the Norwegian South-Eastern regional health authorities via grant numbers 2021039 and 2023059 to S.H., H.L. and E.O.V.M. The funders had no role in study design, data collection and analysis, decision to publish or preparation of the manuscript.

Author contributions

The study was led by F.S. and M. Sill. A.P., K.G., D.S., S. Halldórsson, G.F., M.L., M. Schlesner and M. Sill wrote the code and analyzed data. M.L., S.P. and S.S. led the study in Nottingham. Pathological evaluation was conducted by F.H., H.B., F.S., H.L., S.B. and S.P. Wet-lab experiments were performed by F.H., N.S., J.M., H.K., M.B., M.R., P.G., L.P., S.D., N.H. and I.C. Neurosurgical samples were provided by S.I., S.S., C.H.-M., S.K. and A.U. A.L. assisted with figure preparation. D.S. developed the MNP-Flex website. Data was contributed by P.K., S. Hamelmann, C.B., F.M.I., N.B., P.E., L.S., C.H., N.V.R., J.V.D., J.V.d.M., S.L., F.D., S.W., R.M., H.L., D.M., A.S., M.H., R.G., S.R., J.H., S.F., V.G., N.J., W.W., S.M.P., E.O.V.-M., A.v.D. and D.T.W.J. A.P., F.S. and M. Sill wrote the paper with contributions from all coauthors.

Competing interests

M. Sill, S.M.P., A.v.D., D.T.W.J., D.S. and F.S. are co-founders and shareholders of Heidelberg Epignostix GmbH. A.P. became a full-time employee of Heidelberg Epignostix GmbH in December 2024, while N.J. and M. Sill joined as full-time employees in July 2024, and D.S. became a part-time employee in November 2024. M.L. was a member of the Oxford Nanopore Technologies MinION access program and previously received free flow cells and sequencing reagents. M.L., S.H., H.L. and E.O.V.M. have received reimbursement for travel, accommodation and conference fees to speak at events organized by ONT. A.P., H.K., S.M.P., A.v.D., D.T.W.J., M.L., M. Sill and F.S. are inventors on a patent application related to a nanopore sequencing-based method for cancer characterization, filed by Deutsches Krebsforschungszentrum (DKFZ), Universität Heidelberg, and Oxford Nanopore Technologies PLC (patent application number: 18682016). The other authors declare no competing interests.

Additional information

Extended data is available for this paper at https://doi.org/10.1038/s41591-025-03562-5.

Supplementary information The online version contains supplementary material available at https://doi.org/10.1038/s41591-025-03562-5.

Correspondence and requests for materials should be addressed to Martin Sill or Felix Sahm.

Peer review information *Nature Medicine* thanks Kunal Rai, Jeremy Rich and the other, anonymous, reviewer(s) for their contribution to the peer review of this work. Primary Handling Editor: Anna Maria Ranzoni, in collaboration with the *Nature Medicine* team.

https://doi.org/10.1038/s41591-025-03562-5

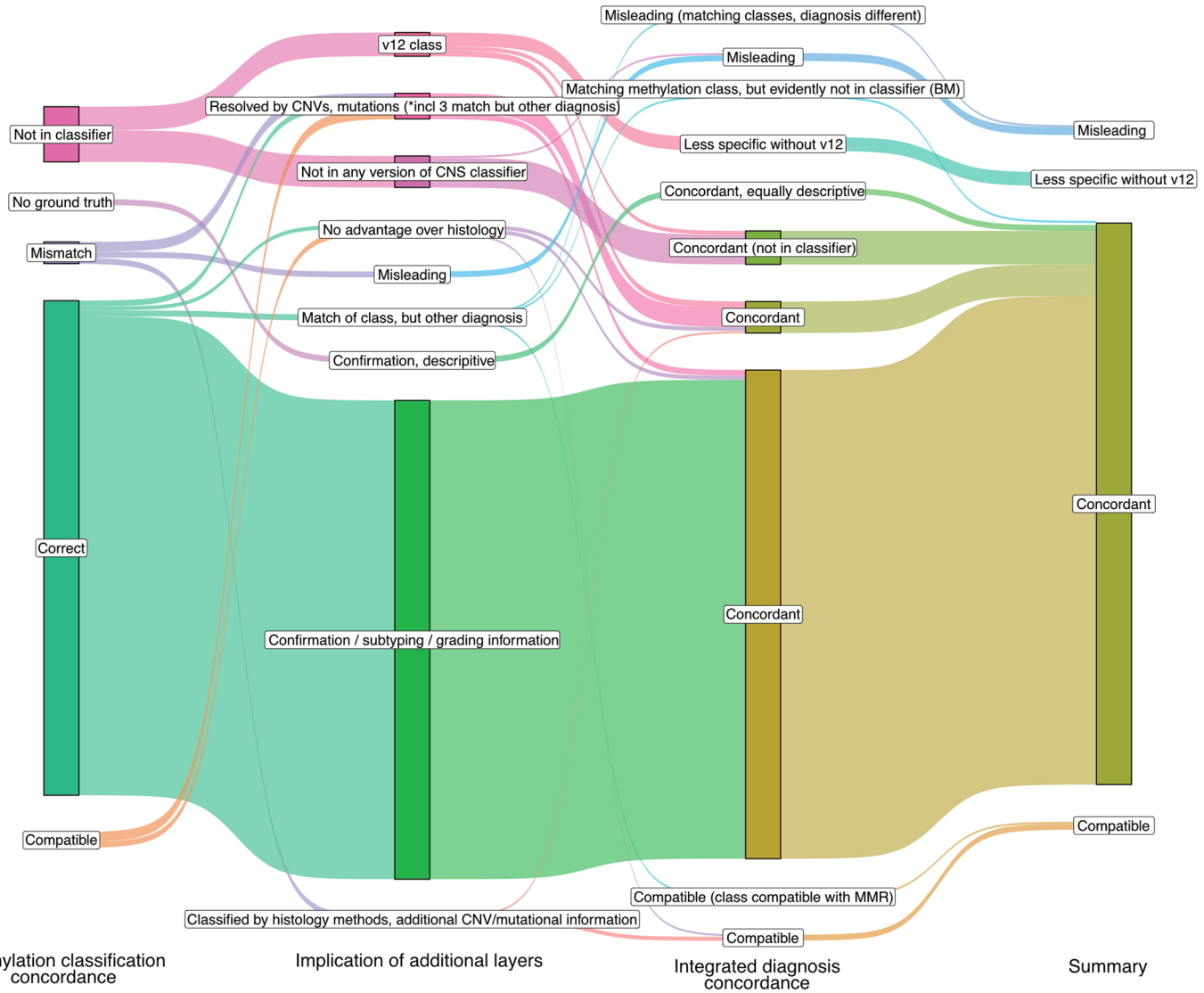

Extended Data Fig. 1 | Summary figure illustrating concordance over levels of evaluation. "*Methylation classification concordance*" is the concordance for methylation classes predicted by Rapid-CNS2. "*Implication of additional layers*" denotes how information like mutations, CNVs, and fusions were used. "*Integrated diagnosis concordance*" indicates concordance of integrated diagnosis by Rapid-CNS[2] derived data to that obtained using conventional methods. "*Summary*" is the summary of concordance.

https://doi.org/10.1038/s41591-025-03562-5

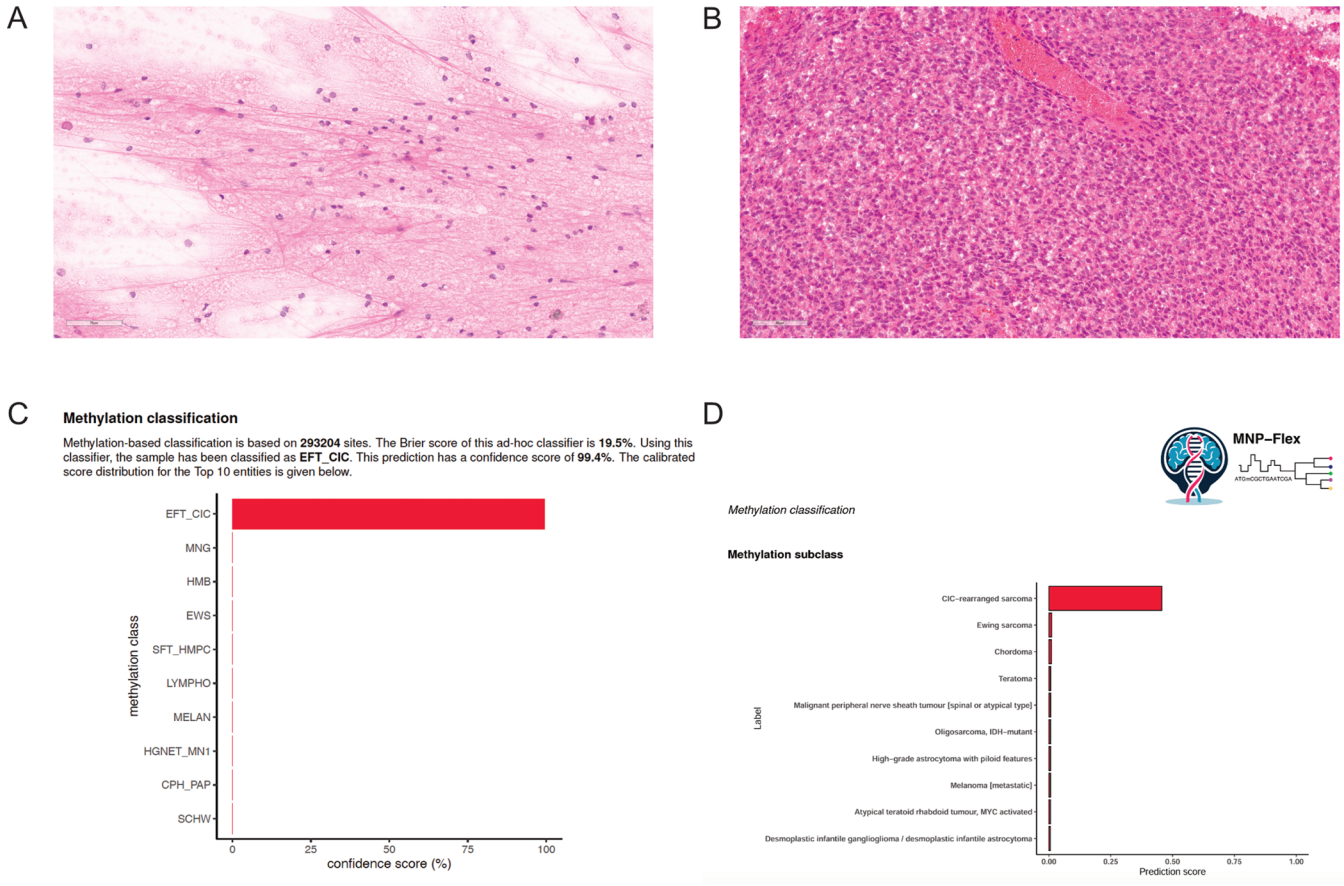

Extended Data Fig. 2 | Rapid molecular reclassification of a suspected glioma. Representative regions from **A**) Smear H&E stain and **B**) frozen H&E section for Study ID 212. H&E slides were inspected by two pathologists independently and both suspected the sample to be a glioma in the intraoperative frozen section diagnosis. **C**) Rapid-CNS[2] predicted it to be a EFT_CIC (CIC altered Ewing family tumour) within 30 minutes of sequencing and after 24 h of sequencing. **D**) MNP-Flex methylation classification after 24 h of sequencing indicated it to be a CIC-rearranged sarcoma. **E**) Rapid-CNS[2] and **F**) EPIC array copy number profiles after 24 h of sequencing.

https://doi.org/10.1038/s41591-025-03562-5

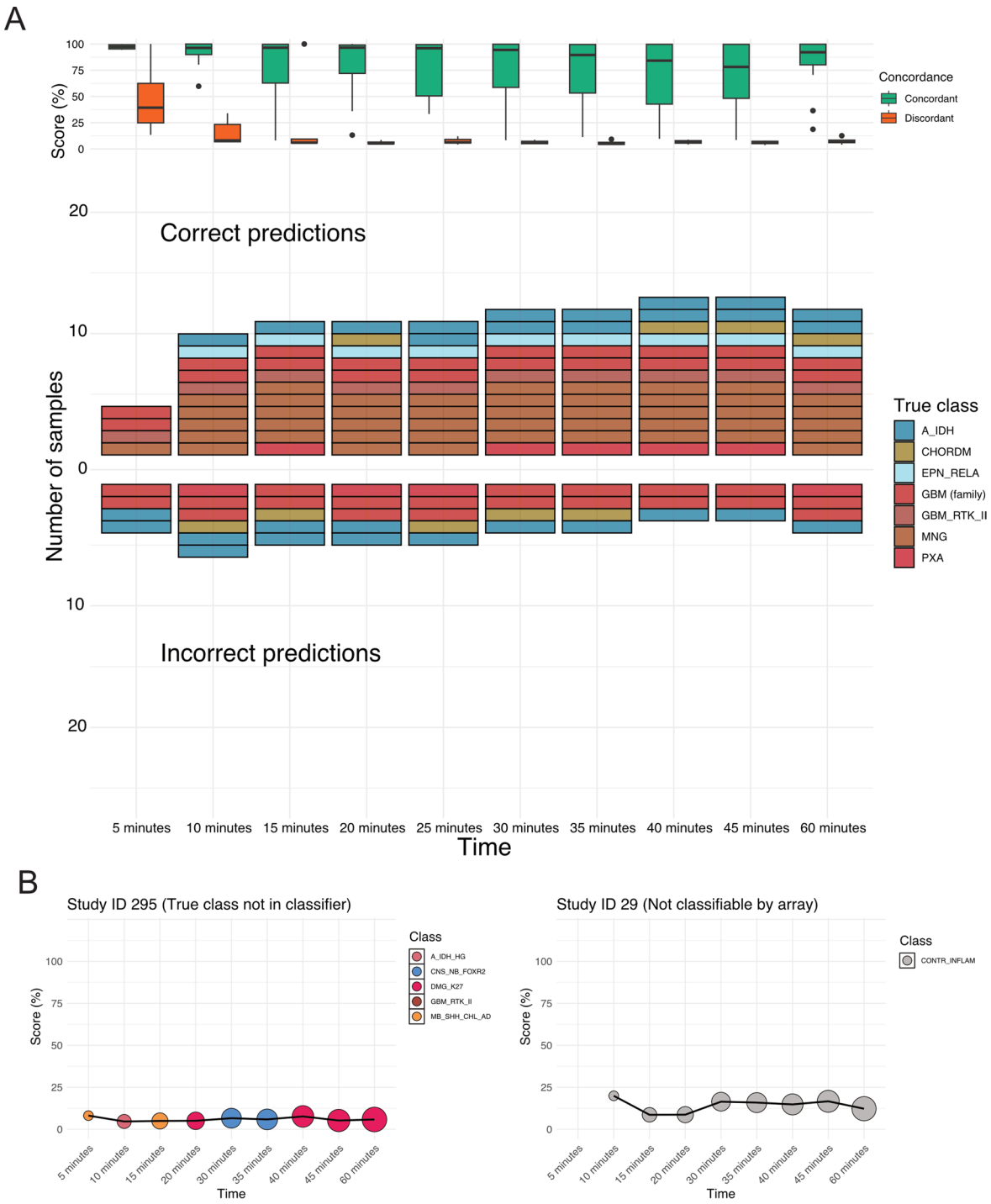

Extended Data Fig. 3 | Intraoperative sequencing and classification reporting. **A**) Rapid-CNS[2] methylation class predictions over 1 hour of sequencing time for 16 classifiable samples from the 18 intraoperative runs. Boxplots (top) indicate calibrated scores for correct (green) and incorrect (orange) predictions. Box plots show the median (horizontal line) and the box boundaries correspond to the 25th and 75th percentiles (interquartile range). Whiskers extend up to 1.5 times the interquartile range beyond these boundaries. Any data points outside this range are displayed individually as outliers. The number of samples represented in each box plot matches the sample counts shown in the accompanying bar plots. (bottom) Each rectangle on the bar plot indicates individual samples coloured by true methylation class or inferred methylation family (GBM). X axis indicates time in minutes. Positive Y-axis indicates correct predictions, negative Y-axis indicates incorrect predictions for the prediction. **B**) Prediction over time for two unclassifiable samples, not included in A). (left) did not have a true class represented in the classifier and (right) had low (< 0.3) scores for the corresponding methylation array. Both were predicted with low confidence (< 25%).

https://doi.org/10.1038/s41591-025-03562-5

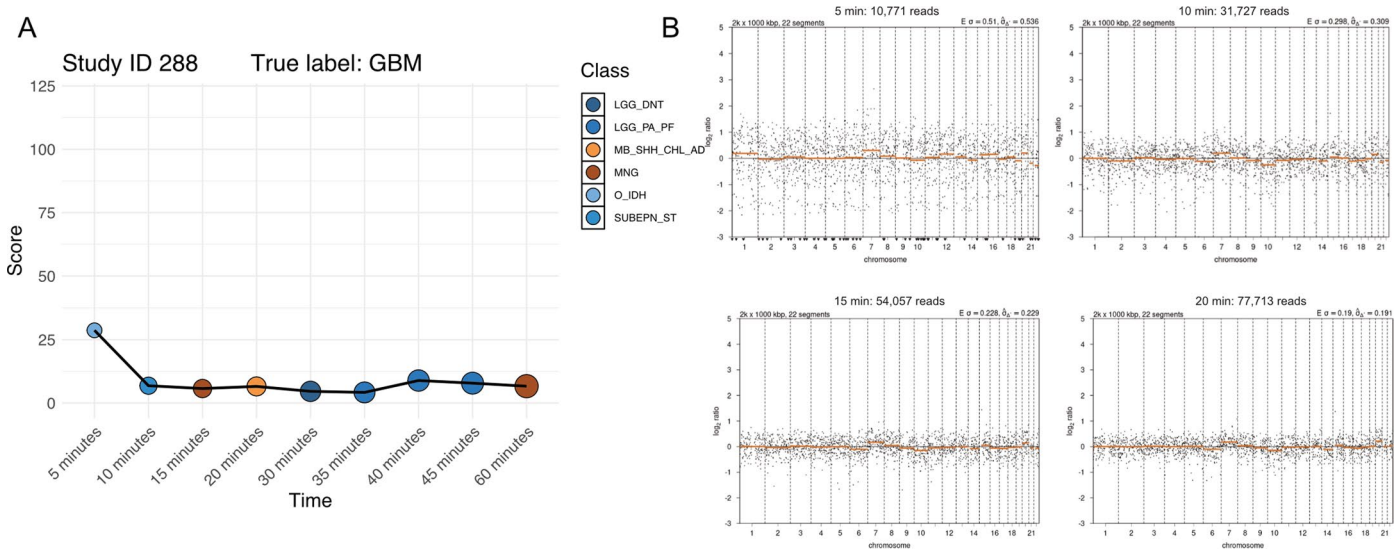

Extended Data Fig. 4 | CNV profiles resolve cases with unclear methylation classification. A) Rapid-CNS[2] methylation class predictions over 1 hour of sequencing time for intraoperative runs. X axis indicates time in minutes and Y-axis indicates score (%) for the prediction. **B**) CNV profiles from 5 to 20 min of sequencing for the samples. Study ID 288 was not correctly predicted by methylation, but displayed a clear chr7 gain / chr10 loss in the intraoperative CNV profiles.

https://doi.org/10.1038/s41591-025-03562-5

Extended Data Table 1 | Accuracies of MNP-Flex validation cohorts

Dataset	*Sample type*	*Cut-off score*	*Subclass-level accuracy*	*Family-level accuracy*	*Confidence interval (subclass)*	*Confidence interval (family)*	*Sample size*
Array-based MNP dataset							
MNP-RF ≥0.7	FFPE/ Cryopreserved	None	92.70%	95.70%	92.5% - 92.8%	95.5% - 95.8%	78,833
		≥0.7	98.50%	99.54%	98.4% - 98.6%	99.49% - 99.59%	58,410
MNP-RF ≥0.9		≥0.7	99.30%	99.70%	99.3% - 99.4%	99.6% - 99.7%	52,735
Non-array dataset							
All non-array (classifiable)	FFPE/ Cryopreserved	None	65.90%	91.90%	61.0% - 70.5%	88.9% - 94.1%	382
		≥0.3	91.10%	99.60%	86.0% - 94.5%	97.6% - 99.9%	215
Whole genome bisulfite sequencing (WGBS)	Cryopreserved	None	93.80%	98.75%	88.15% - 99.03%	96.22% - 100%	80
		≥0.3	94.11%	100%	88.00% - 99.69%	100% - 100%	68
Nanopore whole genome sequencing (ONT-WGS)	Cryopreserved	None	-	100%	-	100% - 100%	40
		≥0.3	-	100%	-	100% - 100%	32
Methylation panels (Twist)	FFPE	None	92.60%	96.29%	82.71% - 100%	89.17% - 100%	27
		≥0.3	100%	100%	100% - 100%	100% - 100%	23
Rapid-CNS2 (Heidelberg)	Cryopreserved	None	66.00%	89.70%	59.31% - 72.65%	85.41% - 93.97%	194
		≥0.3	89.18%	98.64%	82.11% - 96.26%	96.02% - 100%	74
Rapid-CNS2 (Nottingham)	Cryopreserved	None	63.40%	90.20%	48.67% - 78.16%	81.16% - 99.33%	41
		≥0.3	77.78%	100%	58.57% - 96.98%	100% - 100%	18
Whole cohort (array/non-array, classifiable)	FFPE/ Cryopreserved	≥0.7 / ≥0.3	99.20%	99.60%	99.1% - 99.2%	99.6% - 99.7%	58,625

nature portfolio

Corresponding author(s): Prof Dr Dr Felix Sahm

Last updated by author(s): Dec 19, 2024

Reporting Summary

Nature Portfolio wishes to improve the reproducibility of the work that we publish. This form provides structure for consistency and transparency in reporting. For further information on Nature Portfolio policies, see our Editorial Policies and the Editorial Policy Checklist.

Statistics

For all statistical analyses, confirm that the following items are present in the figure legend, table legend, main text, or Methods section.

n/a	Confirmed
☐	☒ The exact sample size (*n*) for each experimental group/condition, given as a discrete number and unit of measurement
☒	☐ A statement on whether measurements were taken from distinct samples or whether the same sample was measured repeatedly
☐	☒ The statistical test(s) used AND whether they are one- or two-sided *Only common tests should be described solely by name; describe more complex techniques in the Methods section.*
☒	☐ A description of all covariates tested
☒	☐ A description of any assumptions or corrections, such as tests of normality and adjustment for multiple comparisons
☐	☒ A full description of the statistical parameters including central tendency (e.g. means) or other basic estimates (e.g. regression coefficient) AND variation (e.g. standard deviation) or associated estimates of uncertainty (e.g. confidence intervals)
☐	☒ For null hypothesis testing, the test statistic (e.g. *F*, *t*, *r*) with confidence intervals, effect sizes, degrees of freedom and *P* value noted *Give P values as exact values whenever suitable.*
☒	☐ For Bayesian analysis, information on the choice of priors and Markov chain Monte Carlo settings
☐	☒ For hierarchical and complex designs, identification of the appropriate level for tests and full reporting of outcomes
☒	☐ Estimates of effect sizes (e.g. Cohen's *d*, Pearson's *r*), indicating how they were calculated

Our web collection on statistics for biologists contains articles on many of the points above.

Software and code

Policy information about availability of computer code

Data collection	No commercial or open source software was used for data collection in this study
Data analysis	Analysis code for different use cases of Rapid-CNS2 and preprocessing code to convert bedmethyl files to MNP-Flex compatible input is available on Github (https://github.com/areebapatel/Rapid-CNS2_sh; https://github.com/areebapatel/Rapid-CNS2_nf). Latest versions of MinKNOW were used as applicable on the devices. Readfish v2024.2.0 was used for intraoperative analysis. Tools used included: Rapid-CNS2 Pipeline: Initial version: Guppy v4.4.0, Megalodon Updated version: Guppy v5+ (basecalling, methylation calling via Remora, alignment). Dorado for basecalling/alignment; modbam2bed v0.5.3 for methylation values; liftover tool, SNV detection: PEPPER-Margin-DeepVariant (r0.4 for R9, r0.8 for R10 flowcells). CNV calling: cnvpytor (v1.2.1 for R9, v1.3.1 for R10 flowcells). Structural variants: Sniffles2 (v2.2), annotated using AnnotSV (v3.0.7). Annotation: ANNOVAR (downloaded May 7, 2021). Subset BAM creation: Bedtools v2.30.0. Methylartist (v1.2.8) for methylation visualization. Alignment: wf-human-variation (ONT pipeline) and Nextflow. Intraoperative Protocols: Real-time analysis: Dorado (dna_r10.4.1_e8.2_400bps_sup), modbam2bed (Heidelberg), and modkit (Nottingham). Nanopore WGS: Basecalling and mapping: MinKNOW (v23.07), Dorado (v7.1.14), wf-human-variation (v1.8.1), modbam2bed (v0.10.0), modkit (v0.2.0). Methylation Array Analysis: Beta-value processing: minfi (v1.21.4), limma (v3.30.11). WGBS Analysis: Methylation analysis: MethylCtools (ODCF Bisulfite core workflow).

MNP-Flex Model:
Machine learning: XGBoost (v2.01) with Caret (v6.0-94).
Visualization: ggplot2 (v3.5.1), ggsankey (v0.0.99999), ggridges (v0.5.4), patchwork (v1.1.3).
Confidence intervals: Binom R-package.
Equivalence testing: TOSTER (v0.8.3).
Twist Panel Sequencing:
Methylation values: nf-core/methylseq (v1.6.1).
Time to Classification:
Basecalling: Guppy v6.4.6 (super accuracy configuration).

For manuscripts utilizing custom algorithms or software that are central to the research but not yet described in published literature, software must be made available to editors and reviewers. We strongly encourage code deposition in a community repository (e.g. GitHub). See the Nature Portfolio guidelines for submitting code & software for further information.

Data

Policy information about availability of data

All manuscripts must include a data availability statement. This statement should provide the following information, where applicable:

- Accession codes, unique identifiers, or web links for publicly available datasets
- A description of any restrictions on data availability
- For clinical datasets or third party data, please ensure that the statement adheres to our policy

Data generated in this study has been uploaded to Zenodo and is accessible at https://doi.org/10.5281/zenodo.13351527. Raw sequencing data will be made available upon reasonable request to Felix Sahm (felix.sahm@med.uni-heidelberg.de). Requests will be reviewed and responded to within 14 working days

Research involving human participants, their data, or biological material

Policy information about studies with human participants or human data. See also policy information about sex, gender (identity/presentation), and sexual orientation and race, ethnicity and racism.

Reporting on sex and gender	Patient sex and/or gender were not considered in the design of the study, and were also not considered in the inclusion criteria. Patient sex was self-reported and available for 239 patients in the Rapid-CNS2 cohort. Age, sex, and/or gender were not included in the study design, as the focus was on validating a platform for molecular profiling. Based on available literature, such profiling accuracy is not known to be influenced by age, sex, or gender.
Reporting on race, ethnicity, or other socially relevant groupings	Patient race, ethnicity and/or other socially relevant groupings were not considered in the design of the study, and were also not considered in the inclusion criteria
Population characteristics	Patients were recruited from the each of the local sites, the only inclusion criteria was suspected CNS tumour with a neurosurgical specimen. No age, sex, gender or ethnicity factors were taken into account.
Recruitment	Archival samples with sufficient cryopreserved tissue were selected for Rapid-CNS2. Diagnostic samples were also similarly recruited if at least 1.5mm diameter tissue was available.
Ethics oversight	This study complied with ethics regulations as approved by the Ethics Committee Heidelberg (S-318/2022), Ethics Committee Nottingham (11/EM/0076), and Ethical Committee, Ghent University Hospital (Clinical Trial Number/IRB B6702021000850). Patients were not compensated for participation. Patient samples were included if they presented with a suspected CNS tumour and had undergone surgery to ensure tissue availability.

Note that full information on the approval of the study protocol must also be provided in the manuscript.

Field-specific reporting

Please select the one below that is the best fit for your research. If you are not sure, read the appropriate sections before making your selection.

☒ Life sciences ☐ Behavioural & social sciences ☐ Ecological, evolutionary & environmental sciences

For a reference copy of the document with all sections, see nature.com/documents/nr-reporting-summary-flat.pdf

Life sciences study design

All studies must disclose on these points even when the disclosure is negative.

Sample size	No sample size calculation was performed. Sample sizes were determined based on the availability of patients presenting with suspected CNS tumors who had undergone surgery, ensuring sufficient tissue for analysis. The sample size is considered adequate as it encompasses a diverse range of CNS tumour subtypes, allowing for robust validation of the Rapid-CNS2 pipeline and the MNP-Flex model across a broad spectrum of real-world cases.

Data exclusions	No data exclusion criteria was set for Rapid-CNS2. For non-IDAT validation samples for MNP-Flex, all samples submitted by collaborating groups were included
Replication	Technical robustness of the Rapid-CNS2 protocol was established by running the protocol in two laboratories- University Hospital Heidelberg and University of Nottingham
Randomization	There were no experimental groups or randomization in the study design
Blinding	As there were no groups, blinding of participants was not necessary in this study. Neuropathologists and scientists performing molecular analyses and evaluation were blinded to the respective results until final concordance analyses

Reporting for specific materials, systems and methods

We require information from authors about some types of materials, experimental systems and methods used in many studies. Here, indicate whether each material, system or method listed is relevant to your study. If you are not sure if a list item applies to your research, read the appropriate section before selecting a response.

Materials & experimental systems

n/a	Involved in the study
☒	☐ Antibodies
☒	☐ Eukaryotic cell lines
☒	☐ Palaeontology and archaeology
☒	☐ Animals and other organisms
☒	☐ Clinical data
☒	☐ Dual use research of concern
☒	☐ Plants

Methods

n/a	Involved in the study
☒	☐ ChIP-seq
☒	☐ Flow cytometry
☒	☐ MRI-based neuroimaging

Plants

Seed stocks	*Report on the source of all seed stocks or other plant material used. If applicable, state the seed stock centre and catalogue number. If plant specimens were collected from the field, describe the collection location, date and sampling procedures.*
Novel plant genotypes	*Describe the methods by which all novel plant genotypes were produced. This includes those generated by transgenic approaches, gene editing, chemical/radiation-based mutagenesis and hybridization. For transgenic lines, describe the transformation method, the number of independent lines analyzed and the generation upon which experiments were performed. For gene-edited lines, describe the editor used, the endogenous sequence targeted for editing, the targeting guide RNA sequence (if applicable) and how the editor was applied.*
Authentication	*Describe any authentication procedures for each seed stock used or novel genotype generated. Describe any experiments used to assess the effect of a mutation and, where applicable, how potential secondary effects (e.g. second site T-DNA insertions, mosiacism, off-target gene editing) were examined.*